Facoltà di Scienze Matematiche, Fisiche e Naturali
Corso di Laurea in Fisica

Tesi di Laurea Magistrale

Study Of A Model Of Quintessence Coupled To Neutrinos

Candidato: Edoardo Carlesi
Relatore Interno: Prof. Enzo Branchini
Relatore Esterno: Dott. Luca Amendola

Marzo 2009

Contents

Acknowledgements

The present work, mostly done in cooperation with the Theoretical Cosmology group of Heidelberg University from May to October 2008, has been made possible by the considerable effort, support and patience of many people, which I would like to thank here. First of all, comes Georg Robbers, for his (almost) private lessons in C++, cosmology and *vor allem* CMBEASY, which were the cornerstone of this thesis; not to mention all the discussions and fundamental explainations during my stay in Heidelberg. Vielen Dank!

Then, of course, come my advisors Luca Amendola and Enzo Branchini, for the patience in reading and correcting this work, the useful discussions but most important for delivering me interest into cosmology during their lectures at Roma Tre.

I would also like to thank Valeria Pettorino, Nico Wintergerst, Lily Schrempp, Miguel Zuma and all the other students, docs and post-docs I met at the theoretical cosmology group of the Institut fuer Theoretische Physik at the Ruprecht-Karls Universitaet Heidelberg, for the interesting discussions and the good time; Sarah Folkerts and Richard Schmidt *fuer die bequemigkeit*; Jennifer May for the great opportunity of learning and earning; Robert, Anna, Nina, Melissa, Matthias, Enikoe, Milena, Manfred und Tilly, Annika, Roberta S., Lucia, Alberta und Angelo for the *Gastfreundschaft*; my family for the - not only financial - support in Heidelberg and during all the years of my physics studies; my friends and collegues here at Roma Tre University: Karkar, Beo, Yasser, Socci, Mike, Jimbo, Borsone and all the others - they're just too many to mention here - and last but not least my dear Roberta, for her neverending patience and love.

Edoardo

Chapter 1

Introduction

The observation of the accelerated expansion of the universe - dating back to 1998-1999, when the seminal works [31],[32], [60] by Riess and Perlmutter were published - stands as a milestone in the development of the modern cosmological paradigm.

Undoubtedly, this can be considered one of the most important turning points in cosmology, together with the discoveries of the universe expansion (Hubble, 1929) and the Cosmic Microwave Background (Penzias and Wilson, 1967).

In fact, as these produced a revolution in the way the universe was described (the former reversing the idea of a static cosmos, the latter providing decisive evidence in favour of the Big Bang Model); so did the type I-a supernovae (SNe Ia) observations, shifting the paradigm to the actual ΛCDM model where Λ, the ill-famous Einstein's cosmological constant, has been reintroduced in the field equations in order to explain the *accelerated* expansion of the universe.

The existence of such a constant energy density could be naivey explained in the frame of a fundamental Quantum Field Theory, whose non-zero ground state energy should be a natural candidate for the explanation of an ubiquitous negative-pressure fluid. Unfortunately, the incredible discrepancy (more or less, 120 orders of magnitude!) between the required value for Λ and the predicted QFT ground-state, make such an approach (requiring a fine tuning this huge) unsatisfactory from the theoretical point of view [1].

[1] Actually, these models are plagued by another kind of fine-tuning, the so called *why now?* or *coincidence* problem; but we shall talk more in depth about it later on.

This is why many theorists have preferred a totally different approach to the *what is this Cosmological Constant?* problem, which might be summarized in two simple steps: first, assume that the ground energy of the fundamental Quantum Field Theory is zero (due to some hypothetical mechanism related to this yet unknown fundamental theory), second, find a dynamical mechanism to generate a negative pressure fluid (generally called *Dark Energy*), which accounts for the observed accelerated expansion.

Although there's some arbitrariness in this approach as well, it's undeniable that the subsequent theoretical effort has produced more than a handful of interesting models, many of which have solid particle physics motivations and non trivial phenomenological implications.

In this work I will study and analyze in depth the theoretical and observational features of one of these models, where the dark energy (generated by a scalar field called *Quintessence*) is coupled to neutrinos. Some emphasis will be also put on the computational and statistical techniques which have been used throughout the whole work.

In the next sections I will describe the actual Cosmological Standard Model, its experimental foundations, its triumphs as well as its shortcomings. The third chapter will deal with the general properties of Quintessence models, focusing on the ones that make them a viable candidate for Dark Energy. Then, in the fourth chapter, I will finally introduce the coupled neutrino model, discussing its motivations, its features and its phenomenology. The results of the Montecarlo simulations and the likelihood analysis, which considerably constrain the model's parameters and predictions, will be shown and discussed throughout the fifth and sixth chapters. In the end, we'll draw some conclusions on the model's success and failures, and we'll also outline the path for a possible extensions of the model and future developments in the field. In appendix A.1 the C++ program CMBEASY, on which most of the results here presented rely, will be extensively described.

Chapter 2

The Standard Cosmological Model

2.1 Theoretical Foundations

The cornerstone of the standard cosmological model is the so called *cosmological principle*, which can be easily stated as follows: *the Universe is homogeneus and isotropic*; which means basically that there's no preferential point of observation in the Universe, and that its components have the same density everywhere. Altough this second statement is clearly false on small scales, on sufficently large ones it is accurate enough to justify its use.

The second fundamental ingredient in the SM are the Einstein field equations, which are derived from the General Relativity Theory:

$$T_{\mu\nu} = \frac{8\pi G}{3}(R_{\mu\nu} - \frac{1}{2}g_{\mu\nu}R) \tag{2.1}$$

and describe the effects of gravitation (due to the $T_{\mu\nu}$ stress-energy tensor) in terms of space-time geometry (the Ricci tensor $R_{\mu\nu}$).

Without any further assumption, these tensor equations are in principle very difficult to solve exactly, since they are non linear [1]. The Cosmological Principle allows a great deal of simplification, since the metric of an homogeneous and isotropic universe is the so-called *Friedmann-Robertson-Walker metric*:

$$ds^2 = g_{\mu\nu}dx^\mu dx^\nu = dt^2 - a(t)^2\left(\frac{dr^2}{1-kr^2} + rd\theta^2 + r^2\sin^2\theta d\phi^2\right) \tag{2.2}$$

[1]Physically, this non linearity is due to the fact that, carrying both energy and momentum, the gravitational field acts as a self-interacting source

where the k, the curvature parameter, can assume the values $0, +1, -1$ [2].

From the Einstein equations combined with a FRW-metric we obtain the *Friedmann equations*:

$$H^2 = \frac{8\pi G}{3}\rho_{tot} \tag{2.3}$$

$$\frac{\ddot{a}}{a} = -\frac{4\pi}{3}(\rho_{tot} + 3p_{tot}) \tag{2.4}$$

which in turn imply the continuity equation:

$$\dot{\rho}_i + 3H(p_i + \rho_i) = 0, \quad i = b, CDM, \nu, \gamma ... \tag{2.5}$$

where we recall that $H = \frac{\dot{a}}{a}$ is the Hubble parameter.
This set of equations describe the dynamics of an homogeneous and isotropic universe. Since an arbitrary number of differently behaving components could be (at least in principle) present, the measure of the global fluid content can be considered as one of the most important tasks of experimental cosmolgy, as it allows us to deterministicallty reconstruct the evolution of the universe and to predict its evolution.

2.2 Experimental Foundations

The ΛCDM Standard Model has so far achieved an incredible success in explaining data coming from the most different areas in observational cosmology into a coherent (although by many points of view incomplete) theoretical framework. Therefore, we're going to describe in a self-consistent manner the way these experiments have been carried and how they provide evidence for the current cosmological model, emphasizing those whose outcomes will be used in the subsequent sections of this work to test the coupled neutrino quintessence model.

2.2.1 Supernovae Observations

As briefly mentioned in the introduction, the biggest evidence for an accelerated expansion of the universe emerged a decade ago, when the first high-precision data on the luminosity distance from SNe Ia-type supernovae were published. The importance of the type Ia supernova relies on the fact that, after their light curves are calibrated, they can be used as *standard*

[2] In the SM it is assumed to be 0, a value which is consistent with observations and is explained in the frame of inflationary models

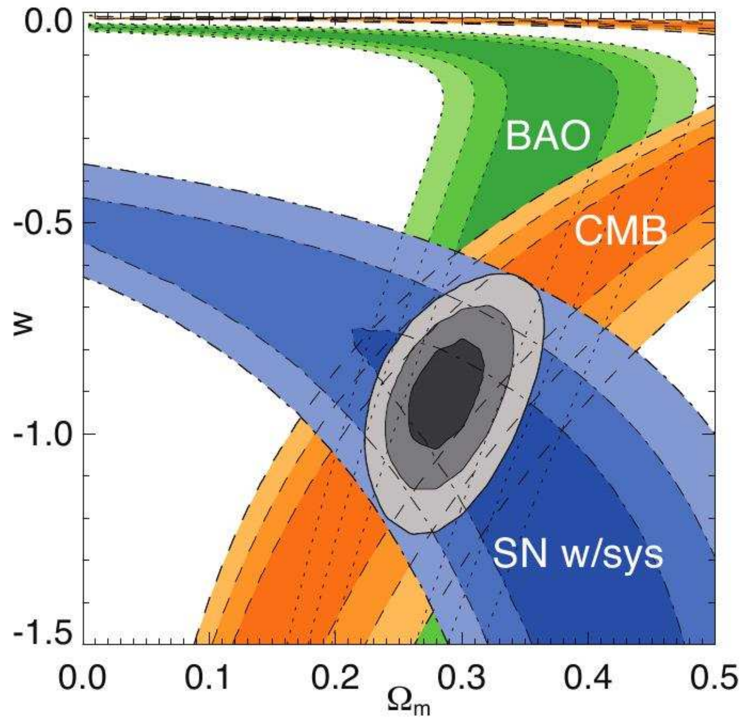

Figure 2.1 — Combined confidence intervals from SNe Ia, BAO and CMB datasets for a constant equation of state w versus Ω_m. Differently shaded regions correspond to the 68%, 95% and 98% confidence level [35].

candles, i.e. their physical properties (most notably, the intrinsic magnitude M) are the same no matter what their redshift is.

Before discussing the issue any further, let us introduce the *luminosity distance* definition:

$$d_L^2 = \frac{L_s}{4\pi\Phi_E} \tag{2.6}$$

where the observed energy flux Φ_E is related to the emitted luminosity L_s by an inverse square geometrical relation [3].

The above relation can be turned into an explicit form for the $d_L(z)$. To do that, we note that, the absolute luminosity L_s and the observed one, L_0, are by definition:

[3]We emphasize that this is just one of the possible definitions of distance in cosmology. For instance, depending on the type of measure, we could use the *comoving* or the *physical* distances

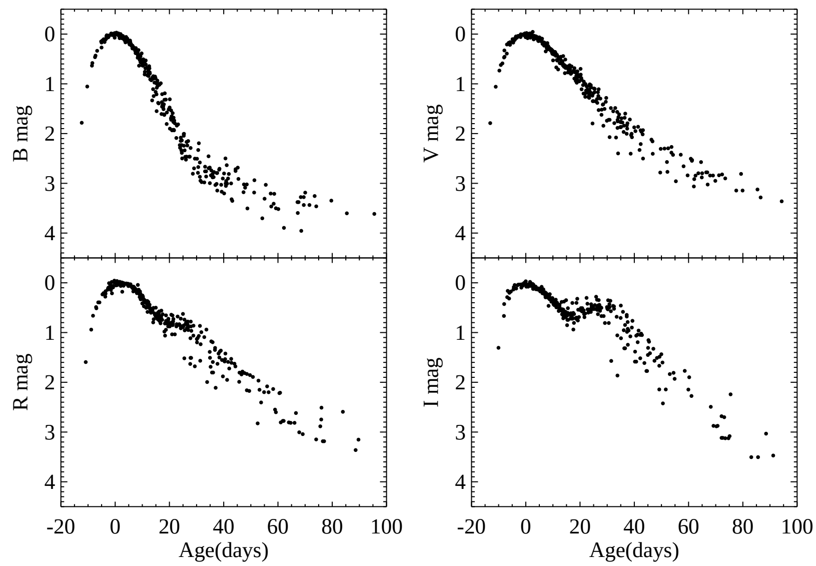

Figure 2.2 — Typical Supernovae Ia luminosity curves [32]

$$L_s = \frac{\Delta E_s}{\Delta t_s}; \quad L_0 = \frac{\Delta E_0}{\Delta t_0} \tag{2.7}$$

that, keeping in mind $\Delta E \sim \Delta \nu$ and $\frac{\nu_s}{\nu_0} \sim 1 + z$, yield:

$$L_s = L_0(1+z)^2 \tag{2.8}$$

which in turn can be combined with the geodesic equation:

$$ds^2 = 0 = dt^2 - a^2(t)dr^2 \tag{2.9}$$

and the Friedmann equation 2.3 to obtain:

$$d_L = \frac{1+z}{H_0} \int_0^z \frac{dz'}{\sqrt{\sum_i \Omega_i (1+z')^{3(1+w_i)}}} \tag{2.10}$$

which explicitly relates the d_L to the matter content of the Universe.

Now, the luminosity distance is related to the apparent magnitude by the relation:

$$m - M = 5\log_{10}(\frac{d_L}{Mpc}) + 25 \tag{2.11}$$

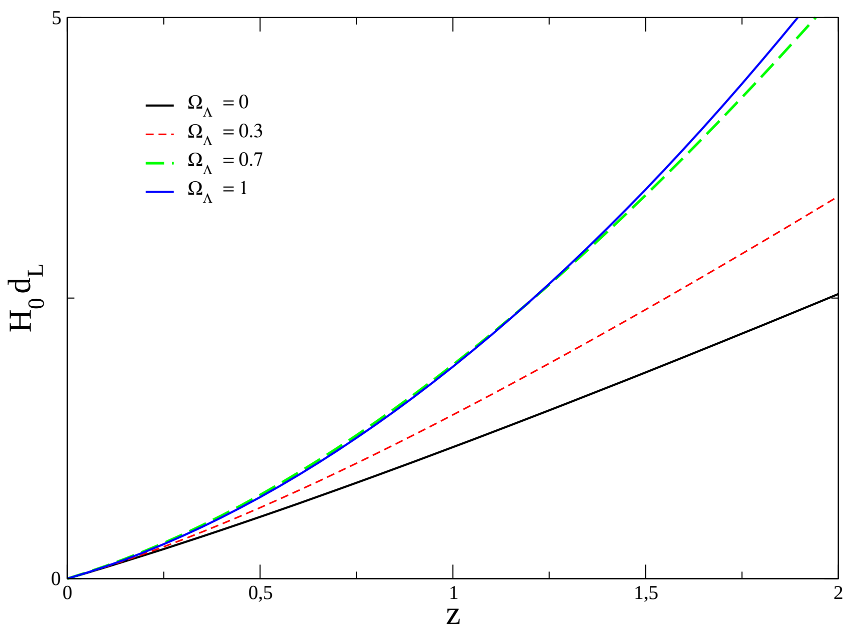

Figure 2.3 — Theoretical luminosity distance versus redshift for different matter content in a flat Universe with two components $\Omega_m + \Omega_\Lambda = 1$

where the numerical factors are due to astronomical conventions in the measure of m and M.

The fact that type Ia supernovae share the same absolute magnitude M allows us to reconstruct the d_L at different redshift from a simple measure of the apparent magnitude m and therefore from 2.10 to infer the total matter content of the universe. The latest analysis on combined SN Ia datasets [38] give for the total matter density the following best fit value:

$$\Omega_m = 0.287^{+0.029+0.039}_{-0.027-0.036} \tag{2.12}$$

where the statistical and systematical uncertainties are separated.

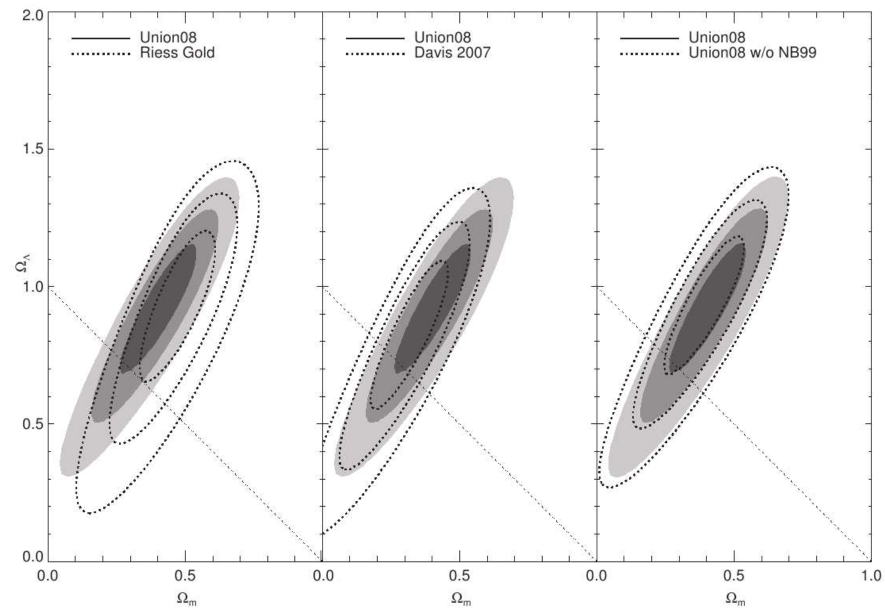

Figure 2.4 — Confidence intervals for the Ω_m and the Ω_Λ. While the first two graphs compare the analysis of [38] to the previous ones carried by Riess *et. al.* [33] and Davies *et. al.* [39] the third one shows the impact of the SCP Nearby 1999 data.

2.2.2 The Cosmic Microwave Background

Further striking evidence for the ΛCDM model is provided by the CMB anisotropy measurements, which started in late 1989 with the pioneering satellite COBE (*COsmic Background Explorer*) and continued through the years with ground based (CBI, ACBAR) and baloon (BOOMERANG) missions until the advent of WMAP (*Wilkinson Microwave Anisotropy Probe*), whose first results appeared in 2003 (WMAP-1) and who subsequently released updates in 2006 (WMAP-3) and 2008 (WMAP-5). The latter data have made available to the scientific community an unprecedented tool in model selection, which is likely to be improved in the next years by the Planck satellite, which is scheduled to be launched soon. These measurements aim at giving a detailed map of the tiny temperature anisotropies (as small as 10^{-4}) of the microwave background cosmic radiation, whose frequency distribution is that of a perfect black body at $T = 2.75K$. The observed intensity and location of the different anisotropy peaks provide fundamental information on the physical properties of the universe; in particular, on those related to the time it becomes optically thin.

Multipole Expansion

To compare and extract information from the temperature anisotropy sky maps we first have to provide a coherent and effective mathematical framework for our analysis. This is straightforwardly achieved by expanding the function $\frac{\Delta T}{T}(\theta, \phi)$ into spherical harmonics:

$$\frac{\Delta T}{T}(\theta, \phi) = \sum_{l=0}^{\infty} \sum_{m=-l}^{l} c_l^m Y_l^m(\theta, \phi) \tag{2.13}$$

which, using the orthogonality relations for Legendre polynomials, can be rewritten as:

$$c_l^m = \int_{\Omega} \frac{\Delta T}{T}(\theta, \phi) Y_l^{m*}(\theta, \phi) d\Omega \tag{2.14}$$

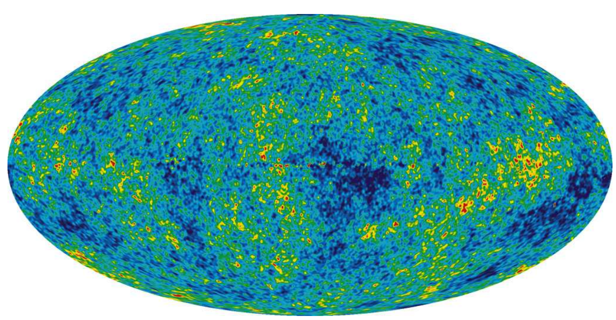

Figure 2.5 — The full-sky map of the temperature fluctuations as seen by the WMAP satellite

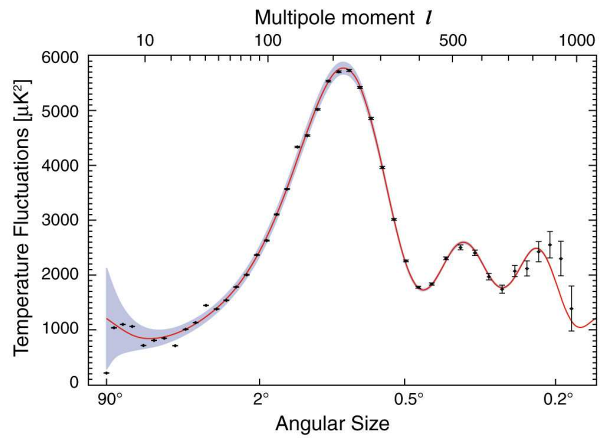

Figure 2.6 — The angular size of the temperature fluctuations measured by WMAP. The solid red line stands for a concor dance ΛCDM model.

These coefficients represent the intensity of the temperature anisotropy $\frac{\Delta T}{T}$ at a given angular scale.

Effects on the CMB

We can observe five different effects on our spectrum, namely:

The Sachs-Wolfe effect occurs because the photons being emitted inside a matter overdensity, have to climb a gravitational potential and are therefore red-shifted: this can be observed on very large scales corresponding roughly to 1°[64].

The acoustic effect is due to the oscillations in radiation and matter; that, at this stage, are strongly coupled and behave like a single component. This effect is responsible for the big anisotropy peaks which can be observed at scales smaller than the Jeans lenght, i.e., smaller than 1°.

The adiabatic initial conditions $\delta_\gamma = \frac{4}{3}\delta_c$, set the initial amplitudes of the photon perturbations.

The Sunyaiev-Zeldovich effect results in an energy increase because of the CMB photons travelling through hot plasma.

The integrated Sachs-Wolfe effect occurs when the gravitational potential driving the perturbations is not constant. In fact, in this case photons may enter a potential well (getting therefore blueshifted) which may deepen in time causing a net loss of energy (i.e. redshift) to the photon. The estimation and analysis of this particular effect are of great relevance in the present work.

The first three phenomena happen during radiation decoupling, while the last two happen along the photon geodesic from decoupling era to present times. The former effects are washed out on very small scales (approximately 4', co rresponding to the last scattering surface's thickness).

2.2.3 Other Observations

More valuable information on our models can be obtained by a large number of different astrophysical and cosmological observations; namely, measures of the *Large Scale Structure Surveys*, *Baryon Acoustic Oscillations*, *Weak Lensing Effects* and *Oldest Stellar Populations Ages* give us tight constraints on the Universe's galaxy clustering pattern, matter content and ages. Anyway, for the pourpose of the present work it will be enough to list them without entering into further detail.

2.3 Open Problems

The list of experimental data which has been so far presented is in remarkable agreement with the ΛCDM model, where the universe's missing dark energy is simply due to a negative pressure fluid with constant equation of state (defined as $p_f = w\rho_f$ where $w = -1$). As already noted, such a component arises naturally in the frame of a fundamental quantum field theory as the vaccum energy density. Assuming the Planck mass ($M_p \sim 10^{19}$ GeV) as the fundamental energy scale for such a fundamental theory, we would expect Λ to be of the order of $M_p^4 \sim 10^{112}\text{eV}^4$; while the observed value is $\Lambda \sim 10^{-10}\text{eV}^4$, yielding a discrepancy of more than 120 orders of magnitude!

The results don't get any better even holding the QCD scale ($M_{QCD} \sim 10^2 MeV$) to be the fundamental one or including possible SUSY-induced suppression. So, the puzzling smallness of the cosmological constant scale ($M_\Lambda \sim 10^{-2} - 10^{-3}\text{eV}$) requires an incredible degree of fine-tuning, which doesn't seem (at least for now) to present viable solution from the point of view of particle physics.

A second conceptual problem arises when we consider that the total matter density ($\Omega_m \sim 0.3$) and the dark energy density ($\Omega_\Lambda \sim 0.7$) are roughly

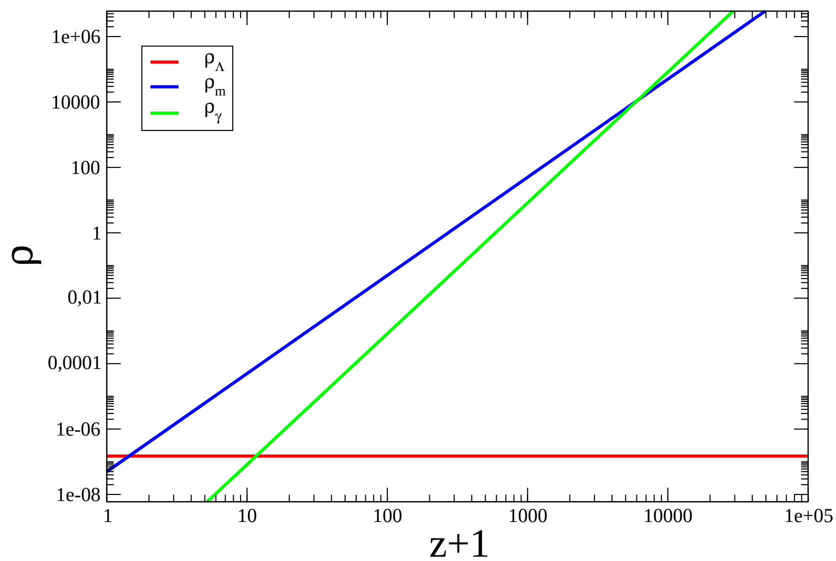

Figure 2.7 — The coincidence problem: why should we be witnessing *now* the transition between two fluids whose e volution is so different and apparently uncorrelated?

of the same order of magnitude, which means that we are in the middle of a transition from a matter-dominated to a dark-energy dominated era: *a priori*, one would consider the occurrence of such an event *now* to be extremely unlikely, again requiring an unnatural fine-tuning of the initial conditions [67]. In fact, if the dark energy were to be constituted by a cosmological constant, the witnessing of a comparable presence in the universe of the densities of matter (changing as $\frac{1}{a^3}$ with the scale factor) and Λ (being costant in time) in this period would seem extremely unlikely.

So, although extremely successful from an experimental point of view, the ΛCDM model seems to be plagued by these two yet unsolved theoretical problems. Quintessence models were born as an attempt to adress them and solve these naturalness issues through a dynamical mechanism.

Chapter 3

Features of Quintessence Models

Although different varieties of scalar-field based approaches have been proposed (like phantoms, K-essence, tachyon and ghost condensates, see [19] for a broad overview on the subject) we will focus in this chapter on quintessence only, which, in its most general definition, is an ordinary scalar field minimally coupled to gravity.

3.1 The Minimally Coupled Quintessence Lagrangian

The action for the quintessence is given by:

$$S = \int d^4x\sqrt{-g}\left(-\frac{1}{2}(\nabla\phi)^2 - V(\phi)\right) \tag{3.1}$$

with $(\nabla\phi)^2 = g^{\mu\nu}\partial_\mu\phi\partial_\nu\phi$ and $V(\phi)$ is the potential of the field, depending on the particular choice of the model. Now, the variation of the action S with respect to the field ϕ gives us the modified Klein Gordon equation:

$$\ddot{\phi} + 3H\dot{\phi} + \frac{dV(\phi)}{d\phi} = 0 \tag{3.2}$$

while the variation with respect to the metric tensor $g_{\mu\nu}$ gives us the energy-momentum tensor:

$$T_{\mu\nu} = \partial_\mu\phi\partial_\nu\phi - g_{\mu\nu}\left[\frac{1}{2}g^{\alpha\beta}\partial_\alpha\phi\partial_\beta\phi + V(\phi)\right] \tag{3.3}$$

In a flat FRW metric we can easily calculate the energy and pressure density of the scalar field:

$$\rho = -T_0^0 = \frac{1}{2}\dot{\phi}^2 + V(\phi) \tag{3.4}$$

$$p = T_i^i = \frac{1}{2}\dot{\phi}^2 - V(\phi). \tag{3.5}$$

The Friedmann equations 2.3 then become:

$$H^2 = \frac{8\pi G}{3}\left[\frac{1}{2}\dot{\phi}^2 + V(\phi)\right] \tag{3.6}$$

and:

$$\frac{\ddot{a}}{a} = -\frac{8\pi G}{3}\left[\dot{\phi}^2 - V(\phi)\right]. \tag{3.7}$$

Equation 3.7 in particular implies that, for $\ddot{\phi}^2 < V(\phi)$ the universe expands with an increasing speed. This slow-rolling condition is satisfied for flat enough potentials. Now, the equation of state for ϕ is given by:

$$w_\phi = \frac{p}{\rho} = \frac{\dot{\phi}^2 - V(\phi)}{\dot{\phi}^2 + V(\phi)} \tag{3.8}$$

which, in the slow-roll regime, yields $w_\phi = -1$. Using the continuity equation 2.5 we can write:

$$\rho = \rho_0 \exp\left[-\int \frac{da}{a} 3(1 + w_\phi)\right] \tag{3.9}$$

that for the above limit reduces to $\rho = const.$, a cosmological constant-like behavior.

3.1.1 Accelerated Expansion Solutions

In order to get accelerated expansion, the $a(t)$ factor must behave (at least) as

$$a(t) \propto t^p \tag{3.10}$$

with $p > 1$. Subtracting the two members of the 3.7 from 3.6 we obtain:

$$\dot{H} = -4\pi G\dot{\phi}^2 \tag{3.11}$$

since:

$$\frac{dH}{dt} = \frac{d\frac{\dot{a}}{a}}{dt} = \frac{\ddot{a}}{a} - \left(\frac{\dot{a}}{a}\right)^2 .$$

The above relation can be rewritten as:

$$\phi = \int dt \left[-\frac{\dot{H}}{4\pi G} \right]^{\frac{1}{2}} . \tag{3.12}$$

Again, from the 3.6 and 3.7 we have an explicit expression for the potential:

$$V = \frac{3H^2}{8\pi G} \left(1 + \frac{\dot{H}}{3H^2} \right) . \tag{3.13}$$

From the condition 3.10 we have the following relations:

$$H = \frac{p}{t}; \quad \dot{H} = -\frac{p}{t^2}; \quad \phi = \sqrt{\frac{p}{4\pi G}} \ln t \tag{3.14}$$

which can be substituted into the 3.13 to give:

$$V(\phi) = V_0 \exp\left(-\sqrt{\frac{16\pi}{p}} \frac{\phi}{M_p} \right) \tag{3.15}$$

remembering that $G \sim M_p^{-2}$. Equation 3.15 shows that scalar field exponential potentials give rise to an accelerated expansion. This is true also for potentials less steep than this one.

In the following paragraphs we'll study in detail the mathematical and physical properties of this as well as of different forms of potential, and, in particular, how they can be adressed to solve the naturalness problems of the cosmological standard model.

3.2 Scaling Solutions in Quintessence Scenario

We now want to study the dynamics of a scalar field ϕ in the presence of a dominant matter component. In this case the Friedmann equations can be written as:

$$H^2 = \frac{8\pi G}{3} (\rho_\phi + \rho_m) \tag{3.16}$$

$$\dot{H} = -4\pi G (\rho_\phi + p_\phi + \rho_m + p_m) \tag{3.17}$$

while the densities obey the conservation equations:

$$\dot{\rho_\phi} + 3H(1 + w_\phi) = 0 \tag{3.18}$$

$$\dot{\rho_m} + 3H(1 + w_m) = 0 \tag{3.19}$$

where w_m is constant (so that matter density scales as $\rho_m = \rho_0 a^{-3(1+w_m)}$) while we assume that w_ϕ can change with time. For the moment, we want to tackle the fine tuning problem so that, for any given initial condition, our scalar field may enter into the so called *scaling regime*, characterized by the relation:

$$\frac{\rho_\phi}{\rho_m} = C \tag{3.20}$$

where C is a positive nonzero constant.

In the scaling regime the scalar field density remains subdominant, mimicking the background during radiation ad matter dominating eras. We also note that, in order to have accelerated expansion, we need the system to exit from this regime: we'll discuss later on some way to achieve such a result. Some more general results on cosmological scaling solutions are provided in appendix C as well as in works like [4], [5], [74], [56] and [69]. In the following section we'll show how this regime arises in particular scalar field dark energy models, solving the autonomous system of equations describing their dynamics.

3.3 Autonomous System of Scalar-Field Dark Energy Models

Consider the Lagrangian density of a minimally coupled scalar field ϕ:

$$L = \frac{1}{2}\dot{\phi}^2 + V(\phi) \tag{3.21}$$

the Friedmann and Klein-Gordon equations read:

$$H^2 = \frac{\kappa^2}{3}\left[\frac{\dot{\phi}^2}{2} + V(\phi) + \rho_m\right] \tag{3.22}$$

$$\dot{H} = -\frac{\kappa^2}{3}\left[\dot{\phi}^2 + (1 + w_m)\rho_m\right] \tag{3.23}$$

$$\ddot{\phi} + 3H\dot{\phi} + \frac{dV}{d\phi} = 0. \tag{3.24}$$

It turns out extremely useful to rewrite these equations in terms of the dimensionless variables [18]:

$$N = \ln a, \quad x = \frac{\kappa\dot{\phi}}{\sqrt{6}H}, \quad y = \frac{\kappa\sqrt{V}}{\sqrt{3}H}, \quad \lambda = -\frac{V_{,\phi}}{\kappa V}, \quad \Gamma = \frac{VV_{,\phi\phi}}{V_{,\phi}^2} \tag{3.25}$$

so that the above equations can be written in the autonomous form:

$$\frac{dx}{dN} = -3x + \frac{\sqrt{6}}{2}\lambda y^2 + \frac{3}{2}x\left[(1-w_m)x^2 + (1+w_m)(1-y^2)\right] \tag{3.26}$$

$$\frac{dx}{dN} = -\frac{\sqrt{6}}{2}\lambda xy + \frac{3}{2}y\left[(1-w_m)x^2 + (1+w_m)(1-y^2)\right] \tag{3.27}$$

$$\frac{d\lambda}{dN} = -\sqrt{6}\lambda^2\left(\Gamma^2 - 1\right)x \tag{3.28}$$

with a constraint equation:

$$x^2 + y^2 + \frac{\kappa^2\rho_m}{3H^2} = 1 \tag{3.29}$$

The equation of state w_ϕ and the fraction of energy density Ω_ϕ can be rewritten as:

$$w_\phi = \frac{p_\phi}{\rho_\phi} = \frac{x^2 - y^2}{x^2 + y^2} \tag{3.30}$$

$$\Omega_\phi = \frac{\kappa^2\rho_\phi}{3H^2} = x^2 + y^2 \tag{3.31}$$

while the total effective equation of state $w_{eff} = \frac{p_\phi + p_m}{\rho_\phi + \rho_m}$ becoming:

$$w_{eff} = w_m + (1-w_m)x^2 - (1+w_m)y^2. \tag{3.32}$$

Accelerated expansion occurs for $w_{eff} < -\frac{1}{3}$.

3.3.1 Stability Analysis

We can see from 3.25 that the case of constant λ corresponds to an exponential potential:

$$V(\phi) = V_0 e^{-\kappa\lambda\phi} \tag{3.33}$$

so that also equation 3.28 is trivially satisfied. Exponential potentials arise very naturally in models of unifications with gravity such as Kaluza-Klein theories, supergravity theories and string theories [72], [69]. Now we have to find the fixed points for the coupled cosmological equations, in order to do that, we'll briefly review some theory and definitions related to dynamical systems.

Dynamical Systems

Given a system of two coupled differential equations:

$$\dot{x} = f(x, y, t), \quad \dot{y} = g(x, y, t) \tag{3.34}$$

A point (x_c, y_c) is called a *fixed point* if it satisfies:

$$(f, g)|_{(x_c, y_c)} = 0. \tag{3.35}$$

A fixed point is said to be an *attractor* if:

$$(x(t), y(t)) \rightarrow (x_c, y_c) \quad t \rightarrow \infty \tag{3.36}$$

To find out whether a *fixed point* is an attractor, we shall study the stability of the system around it; in other words, we have to consider small perturbations:

$$x = x_c + \delta x, \quad y = y_c + \delta y \tag{3.37}$$

and substitute them into equation 3.34:

$$\frac{d}{dN} \begin{pmatrix} \delta x \\ \delta y \end{pmatrix} = M \begin{pmatrix} \delta x \\ \delta y \end{pmatrix} \tag{3.38}$$

where the matrix M can be explicitly written as:

$$M = \begin{pmatrix} \frac{\partial f}{\partial x} & \frac{\partial f}{\partial y} \\ \frac{\partial g}{\partial x} & \frac{\partial g}{\partial y} \end{pmatrix}_{(x=x_c, y=y_c)} \tag{3.39}$$

We can write the most general solution to the system of coupled linear equations using the eigenvalues μ_1 and μ_2 of the matrix M as:

$$\delta x = C_1 e^{\mu_1 N} + C_2 e^{\mu_2 N} \tag{3.40}$$

$$\delta y = C_3 e^{\mu_3 N} + C_4 e^{\mu_4 N} \tag{3.41}$$

where C_1, C_2, C_3 and C_4 are constants of integrations. The solutions to this system can be classified as:

Point	x	y	Existence	Stability	Ω_ϕ	γ_ϕ
a	0	0	$\forall \quad \lambda, \gamma$	Saddle point for $0 < \gamma < 2$	0	–
$b1$	1	0	$\forall \quad \lambda, \gamma$	Unstable node for $\lambda < \sqrt{6}$, saddle point for $\lambda > \sqrt{6}$	1	2
$b2$	-1	0	$\forall \quad \lambda, \gamma$	Unstable node for $\lambda > -\sqrt{6}$, saddle point for $\lambda < -\sqrt{6}$	1	2
c	$\frac{\lambda}{\sqrt{6}}$	$\sqrt{1 - \frac{\lambda^2}{6}}$	$\lambda^2 < 6$	Stable node for $\lambda^2 < 3\gamma$, saddle point for $3\gamma < \lambda^2 < 6$	1	$\frac{\lambda^2}{3}$
d	$\sqrt{\frac{3}{2}} \frac{\gamma}{\lambda}$	$\sqrt{\frac{3(2-\gamma)\gamma}{2\lambda^2}}$	$\lambda^2 > 3\gamma$	Stable node for $3\gamma < \lambda^2 < \frac{24\gamma^2}{(9\gamma-2)}$, stable sprial for $\lambda^2 > \frac{24\gamma^2}{9\gamma-2}$	$\frac{3\gamma}{\lambda^2}$	γ

Table 3.1 — Properties and existence of fixed points for the system of coupled equations 3.26, 3.27, 3.28 with exponential potential and constant λ.

Stable node: $\mu_1 < 0$ and $\mu_2 < 0$

Unstable node: $\mu_1 > 0$ and $\mu_2 > 0$

Saddle point: $\mu_1 < 0$ and $\mu_2 > 0$ (and vice-versa)

Stable spiral: M has negative determinant and μ_1 and μ_2 have negative real parts.

Stable spirals and stable nodes are also attractors.

Fixed points for Quintessence with exponential potentials

Now let's go back to our system of equations 3.26 and 3.27; the eigenvalues of the associated matrix are:

Point (a): $\mu_1 = -\frac{3}{2}(2-\gamma), \quad \mu_2 = \frac{3}{2}\gamma$

Point (b1): $\mu_1 = 3 - \frac{\sqrt{6}}{2}\lambda, \quad \mu_2 = 3(2-\gamma)$

Point (b2): $3 + \frac{\sqrt{6}}{2}\lambda, \quad \mu_2 = 3(2-\gamma)$

Point (c): $\mu_1 = \frac{1}{2}(\lambda^2 - 6), \quad \mu_2 = \lambda^2 - 3\gamma$

Point (d): $\mu_{1,2} = -\frac{3(2-\gamma)}{4}\left[1 \pm \sqrt{1 - \frac{8\gamma(\lambda^2-3\gamma)}{\lambda^2(2-\gamma)}}\right]$

where we have defined new variables $\gamma = 1 + w_m$ and $\gamma_\phi = 1 + w_\phi$.

By definition we have $0 < \gamma < 2$ (w_m can vary from 0 to 1). Looking at the properties of our solutions in 3.1 we see that our equations can have two fixed points, namely, (c) and (d). Substituting the x and y from (c) into 3.32 we obtain $w_{eff} = \lambda^2/3 - 1$; therefore in order to have accelerated expansion the relation $\lambda^2 < 2$ must hold.
In the case of the fixed point (d), from 3.30 we see that $w_\phi = w_m$: this is the case of scaling solutions, since quintessence behaves like the dominant component, even though it cannot account for late-time acceleration.

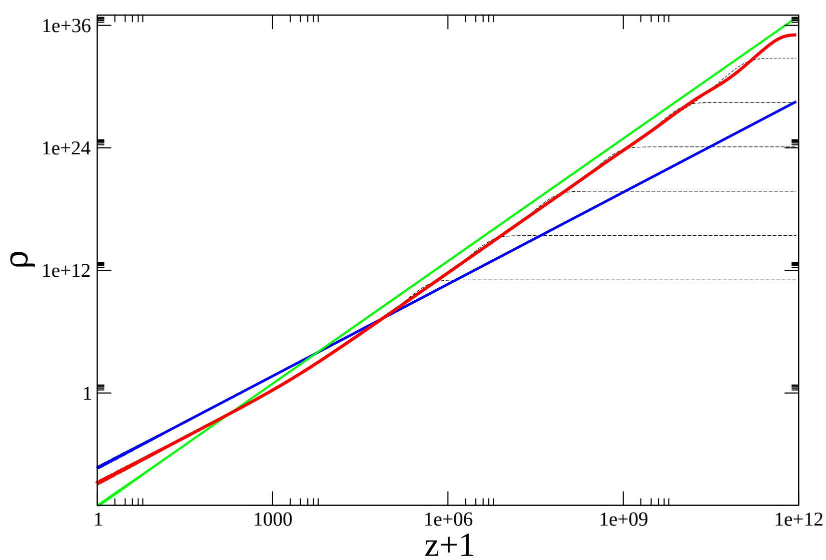

Figure 3.1 — Scaling solutions in uncoupled exponential quintessence: the red solid line is the solution for the field on the radiation attractor, dashed thin black lines are the quintessence densities for different initial conditions while solid blue and green lines are total matter and radiation densities. We see that starting scalar field values don't need to be fine tuned since every solution will enter the scaling regime. This kind of solution, however, does not provide a desired late-time accelerated expansion

In fact, while the constraints on early dark energy require $\lambda \geq 10$, to account for accelerated expansion we should have $\lambda \leq 3$. Therefore, in order

not to give up to the scaling properties, we have to add other ingredients to our model, introducing some modifications to our potentials or allowing the quintessence field to couple.
The first solution can be realized in several different ways. One of these is relaxing the constraint of a constant λ and allowing it to depend on t or ϕ. Another way consists in considering a double exponential potential of the form:

$$V(\phi) = M_p^4 \left[\exp\left(-\frac{\lambda_1 \phi}{M_p}\right) + \exp\left(-\frac{\lambda_2 \phi + \phi_0}{M_p}\right)\right] \tag{3.42}$$

where the constant ϕ_0 is fine tuned so that the first exponential, with a large λ_1, prevails for early times whereas the second one accounts for the late-time Ω_ϕ domination. Acceleration can also be realized within the framework of more general quintessence models, those having non-canonical kinetic terms [44].

3.4 Coupled Dark Energy Models

Probably more interesting are the consequences of a non-minimal coupling between quintessence and matter fields, which, in general, would be accounted for by an effective Yukawa type term of the form:

$$\sum_i F_i(\phi)\bar{\psi}_i\psi_i \tag{3.43}$$

where we sum on different fermion species. As shown in [43], this kind of interaction can arise as the result of quantum corrections to the quintessence potential.

Measures of different materials falling towards the sun constrain such an equivalence principle violating term [63] in the baryon sector to be:

$$F_b < 10^{-24} \tag{3.44}$$

which strongly suppresses any possible interaction between dark energy and ordinary matter. Nonetheless, there's still room left for a coupling in the dark matter or leptonic sector, where present bounds still allow it to take place.

Quite remarkably, it turns out that such a kind of coupling provides new attractor solutions [69], [45], [4], [5] that can provide late time acceleration while preserving the scaling regime for a large portion of cosmic history and thus solving the coincidence problem [56]. Furthermore, interactions of the type 3.43 usually induce time-varying masses, a recurrent feature of most of the coupled quintessence models [12]. Usually, this coupling also implies that only the sum, but not the separate terms, of the energy-momentum tensors for matter and scalar field is conserved:

$$T^{\alpha(m)}_{\beta;\alpha} = -F(\phi)T^{(m)}\phi_{,\alpha} \tag{3.45}$$

$$T^{\alpha(\phi)}_{\beta;\alpha} = F(\phi)T^{(m)}\phi_{,\alpha} \tag{3.46}$$

Anyway, we won't enter now into the details of these models, since our next chapters will be completely devoted to the study of the coupled neutrino scenario, which shares important mathematical and physical properties with most of the interacting quintessence theories.

3.5 Experimental Constraints

To look beyond ΛCDM, we have to search for the signatures of dynamical dark energy that would leave a detectable imprint in observable data. In particular, we have two model-independent quantities that can impose significant constraints (and eventually rule out) our cosmological models: the early amount and equation of state of the dark energy fluid.

3.5.1 Early Dark Energy

While the contribution of a cosmological constant to the total density at early stages would be completely negligible, quintessence scenarios often admit a sizable quantity of dark energy to be present even during early epochs of the universe [24], [16], [9], [27].

Important informations on the amount of early dark energy can be obtained from:

Big Bang Nucleosynthesis: the observed atomic abundances depend on the interplay bewteen interaction rate and expansion of the universe: precise measures of the former considerably constrain the value of the latter, giving us informations on the components which were present at the time.

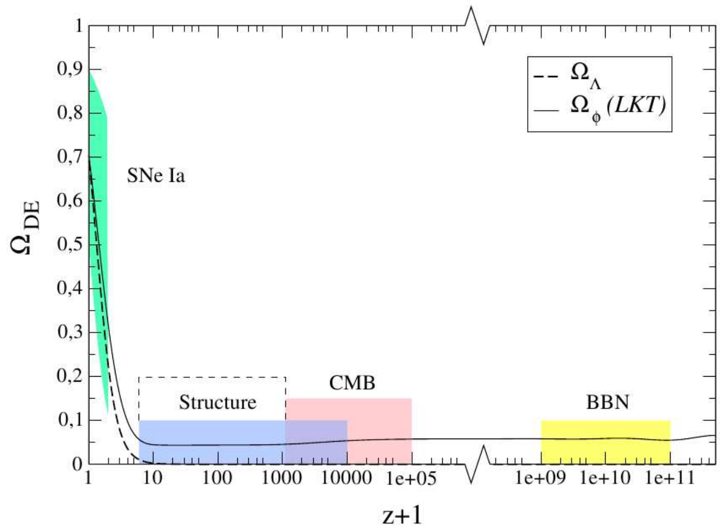

Figure 3.2 — Constraints on Early Dark energy, a Leaping Kinetic Term dark energy is shown against the reference ΛCDM [26]

Structure Formation: a big amount of early dark energy would cause an accelerated expansion which, in turn, would suppress the growth of the structures.

CMB Anisotropies: The height and position of the peaks also is affected by the expansion history of the universe, in particular, by the time of the last scattering and the age of the universe, which depend both on the amount of dark energy.

3.5.2 Equation of State

Supernovae and CMB spectrum measurements are sensitive to the recent expansion history of the universe and can probe the dynamics of dark energy, in particular, constraining the dark energy equation of state w_{DE} [20]. If the dark energy were a cosmological constant, we would expect to observe $w = -1$ at every redshift. On the other hand, if this were not the case, we would have a clear hint of a dynamical dark energy component [70], [22]. Anyway, present bounds are still compatible with a $w = -1$ and cannot provide reliable constraints on its evolution due to large experimental error. Nonetheless we hope that an improved accurracy of these measures will give important informations on the nature of dark energy.

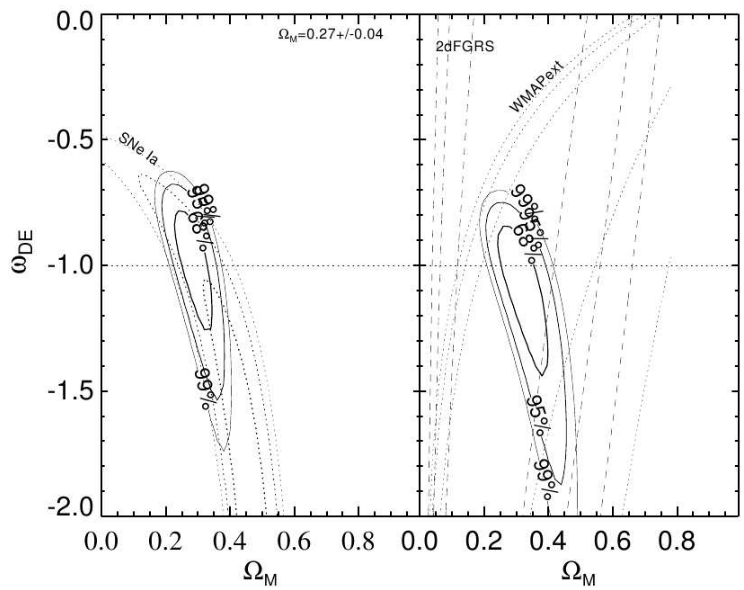

Figure 3.3 — Confidence intervals for the dark energy equation of state from SNe Ia, CMB and LSS measurements [33]

Chapter 4

Neutrinos Coupled to Quintessence

Neutrinos' cosmological key role can be hardly overstimated: almost all of the most recent observations (BBN, CMB anisotropies, LSS, BAO...) provide valuable informations on neutrinos masses and numbers. Since some of the most recent cosmological theories involve neutrinos, it is worth investigating how their properties affect the outcome of observations and can be therefore used for model constraining and selection.

4.1 Cosmic Neutrino Background

Most of the actual role of neutrinos in cosmology is played by the cosmic neutrino backgroud (CNB), i.e. by those neutrinos that, at $T \sim 1MeV$ decoupled from the background evolution and started to freely stream across the universe. Altough no direct evidence for CNB has been found so far, a great number of measures give us indirect proof of the presence of a uniformly distributed neutrino background. This allows us to perform the most precise (better than an order of magnitude, if compared to terrestrial experiments) estimates of neutrino masses.

The importance of this kind of observations relies also in the fact that, differently from solar or nuclear neutrino oscillation measures, they are sensitive to the neutrino absolute mass scale $\sum_i m_{\nu_i}$ (see [49], [75] and [10]) and not simply to the differences $\sum_{ij} \Delta m_{ij}$ between different neutrino flavours, as the standard neutrino oscillations measures are. Moreover, some kinds of observations (like Large Scale Surveys) are in principle dependent on the

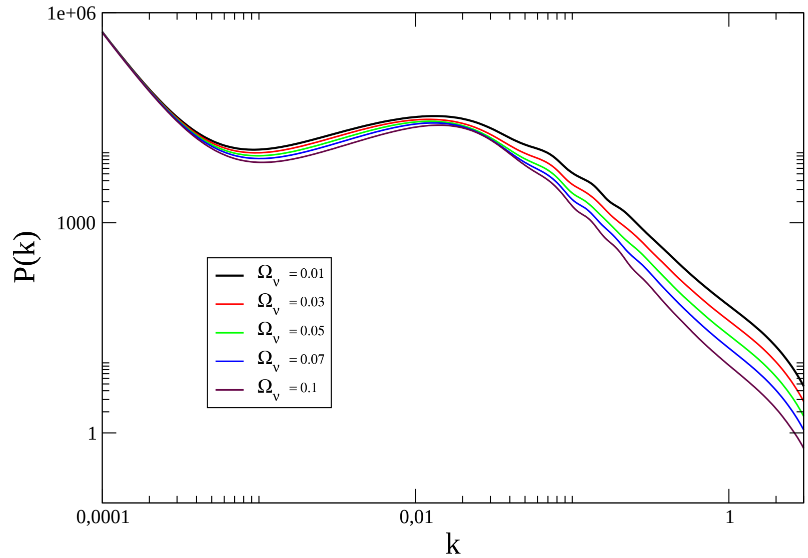

Figure 4.1 — How different neutrino densities affect the matter power spectrum at $z = 0.5$. From the plot it appears that higher densities (and therefore bigger neutrino masses) suppress the clustering of matter on smaller scales. The plot has been calculated with CMBEASY for a standard ΛCMD model in the synchronous gauge.

different masses of each one of the neutrino species [65], so that future high precision detection might determine all of the $m_{\nu i}$.

Neutrino mass scale determines the epoch of the transition from the relativistic to the non relativistic regime, and a change of a few eV in its value can affect dramatically galaxy clustering and structure formation[6]. Although Hot Dark Matter scenario are currently ruled out by LSS (therefore excluding any identification between neutrinos and dark matter), massive νs could nonetheless contribute to dark matter halos mass and properties.

4.2 Massive Neutrinos and CMB Anisotropies

As we can see from fig. 4.2, different neutrino densities have nontrivial effects on the CMB spectrum, since heavier ν_s slightly increase the height of

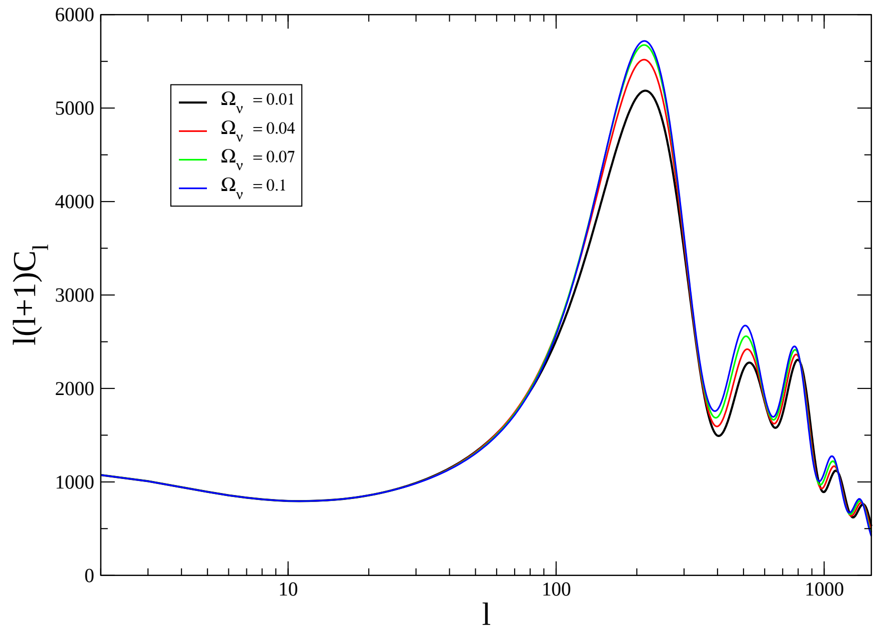

Figure 4.2 — The CMB spectrum calculated for different values of the neutrino density. Ω_Λ is kept fixed while the change in Ω_ν is compensated by a change in Ω_{cdm}

anisotropy peaks. In fact, m_ν of the order of a few eVs (corresponding to $0.01 \leq \Omega_\nu \leq 0.1$) neutrinos would still be relativistic at the time of equality and therefore should be counted as radiation. Indeed, during this epoch we have $\rho_{cdm} + \rho_b = \rho_\nu + \rho_\gamma$, a relation that implies:

$$\begin{aligned} a_{eq}^{-3}(\rho_{cdm}^{(0)} + \rho_b^{(0)}) &= a_{eq}^{-4}(\rho_\nu^{(0)} + \rho_\gamma^{(0)}) \rightarrow \\ a_{eq} = \frac{\rho_\nu^{(0)} + \rho_\gamma^{(0)}}{\rho_{cdm}^{(0)} + \rho_b^{(0)}} & \end{aligned} \tag{4.1}$$

from which we see that the equality is postponed in the case of higher neutrino densities. This means that also the epoch of decoupling takes place later; therefore, perturbations in the strongly coupled photon-baryon fluid can grow for a longer time, enhancing the anisotropy peaks seen on the CMB spectrum. In this way we can highly constrain the value of the neutrino mass, obtaining (at a 95% confidence) from the WMAP data alone[49], [75], [41]:

$$\sum_i m_\nu^{(i)} \leq 2.2\text{eV} \tag{4.2}$$

a limit which can be improved if we take into account other cosmological datasets [52].

4.3 Mass Varying Neutrinos

A link between mass-varying neutrinos and dark energy was proposed by several authors (see [40], [13], [46]), starting from the idea that the similarity between energy scales of the cosmological constant ($\Lambda \sim 10^{-2} - 10^{-3}$eV) and of neutrinos ($m_\nu \sim 10^{-1} - 10^{-3}$) is not a coincidence, but rather the result of some kind of interaction. Fardon, Nelson and Weiner [40] proposed a model in which neutrino mass arises as a result of the coupling with a scalar field A (*Acceleron*) whose potential V depends on m_ν.

Takig the non-relativistic limit ($m_\nu < k$) for the standard expression for the neutrino contribution to the total energy density:

$$E_\nu = \int \frac{d^3k}{(2\pi)^3} \sqrt{k^2 + m_\nu^2} f_\nu(k) \tag{4.3}$$

we have $E_\nu \sim n_\nu m_\nu$. Therefore, we can write an effective potential:

$$V(m_\nu) = m_\nu n_\nu + V_0(m_\nu) \tag{4.4}$$

where $V_0(m_\nu)$ is the scalar field potential.

The equation of state of the total energy density in the neutrino-dark energy sector is:

$$w + 1 = -\frac{m_\nu V_0'(m_\nu)}{V} \tag{4.5}$$

from which we see that:

(a) it is the coupled fluid that accelerated expansion, and not the scalar field alone (like in most of quintessence models)

(b) in order to have a $w \sim -1$ (as required by observtions) either we have a fairly flat $V_0(m_\nu)$ potential or neutrinos have a very small density compared to the dark energy sector.

Some authors claim that this kind of model may give rise to instabilities [1], however, this issue is still under debate [11]. An instability-free coupled neutrino model, which combines some of the features that we outlined here with some others taken from coupled dark energy dark matter models [45], will be introduced in the following section and deeply investigated throughout the rest of the present work.

4.4 Growing Neutrinos

The growing neutrino model was first proposed by Amendola, Baldi and Wetterich [3] as another attempt to solve the naturalness problems of the standard model, combining some aspects of coupled quintessence as well as others from the previously discussed mass varying neutrinos models.

In this scenario, neutrinos couple through their mass to the scalar field:

$$m(\phi) = m_0 e^{-\beta \frac{\phi}{M_p}} \tag{4.6}$$

so that the overall density goes like:

$$\rho_\nu = \rho_{\nu 0} a^{3(\gamma-1)}, \quad \gamma > 1 \tag{4.7}$$

The main feature of this model is that neutrinos play the role of a density-growing matter component (for a negative value of β), which triggers the onset of dark energy domination at $z \sim 0.5$.

The scalar field Lagrangian can be written as:

$$L = \int d^4x \sqrt{-g} \left(g^{\mu\nu} \frac{1}{2} \partial_\mu \phi \partial_\nu \phi + V(\phi) + m_\nu(\phi) \bar{\psi} \psi \right) \tag{4.8}$$

and we assume a standard exponential form for the potential:

$$V(\phi) = M_p^4 e^{-\alpha \frac{\phi}{M_p}} \tag{4.9}$$

The presence of an interaction between quintessence and neutrinos modifies the Klein-Gordon equation:

$$\phi'' + 2\mathcal{H}\phi' = -a^2 \frac{\partial V}{\partial \phi} + a^2 \frac{\beta(\phi)}{M_p} (1 - 3w_\nu) \rho_\nu \tag{4.10}$$

where the $'$ denotes a derivative with respect to the conformal time $d\tau = dt/a$ and $\mathcal{H} = aH$ is the Hubble constant in terms of the conformal time variable. The term $\propto \beta \rho_\nu (1 - 3w_\nu)$ counteracts and eventually stops the evolution of the field when neutrinos become nonrelativistic, i.e. $w_\nu = 0$ whereas their influence is negligible during the relativistic era when $w_\nu = \frac{1}{3}$. The conservation equation for the growing neutrinos and for the scalar field is:

$$\rho'_\phi = -3\mathcal{H}(1+w_\phi)\rho_\phi + \beta(\phi)\phi'(1-3w_\nu)\rho_\nu \tag{4.11}$$
$$\rho'_\nu = -3\mathcal{H}(1+w_\nu)\rho_\nu - \beta(\phi)\phi'(1-3w_\nu)\rho_\nu \tag{4.12}$$

which have the same form of the general equation for the conservation of the sum of the energy momentum tensors 3.45.

4.4.1 Scaling Behaviour

In this section we'll briefly show some of the most remarkable effects of our model, constraining our analysis to the particular case where the coupling β is a constant. As long as neutrinos are relativistic (during radiation and most of matter domination eras) the scalar field follows a tracker solution [68], with a constant fraction of early dark energy:

$$\Omega_\phi = \frac{n}{\alpha^2} \tag{4.13}$$

with $n = 3(4)$ for matter (radiation). This simple behaviour is guaranteed by the intermediate attractor solution (d) of table 3.1; we recall that in the notation we used we had:

$$\Omega_\phi = \frac{8\pi G}{3}\left(\frac{1}{2}\dot{\phi}^2 + V(\phi)\right) = x^2 + y^2 \tag{4.14}$$

where the dimensionless variables x and y were defined in 3.25. If we now take (d), which in terms of these variables was given by:

$$x = \sqrt{\frac{3}{2}}\frac{\gamma}{\alpha}, \quad y = \sqrt{\frac{3(2-\gamma)\gamma}{2\alpha^2}} \tag{4.15}$$

and substitute it into 4.14 we obtain:

$$\Omega_\phi = \frac{3}{2}\frac{\gamma^2}{\alpha^2} + \frac{3}{2}\left(\frac{\gamma(2-\gamma)}{\alpha^2}\right) = \frac{3\gamma}{\alpha^2} \tag{4.16}$$

Since γ was defined as:

$$\gamma = 1 + w_n; \quad n = m, \gamma \tag{4.17}$$

knowing that $w_m = 0$ and $w_\gamma = \frac{1}{3}$, we see that 4.16 reduces to 4.13. When neutrinos are relativistic, the term $\beta(1-3w_\nu)\rho_\nu$ is negligible (since $w_\nu \simeq \frac{1}{3}$) and the 4.10 has the simple solution:

$$\phi = \phi_0 + \frac{2M}{\alpha}\ln\left(\frac{t}{t_0}\right) \tag{4.18}$$

We can easily verify that, during the scaling regime, the following relations hold :

$$\begin{aligned} m_\nu \sim \ \Omega_\nu &\sim t^{2(\gamma-1)}, \\ \rho_\nu &\sim t^{2(\gamma-2)}, \\ \rho_c \simeq \rho_n + \rho_\phi &\simeq \rho_\phi(1+1/\alpha^2) \simeq V(\phi) \end{aligned} \tag{4.19}$$

Equations 4.18 and 4.19 can be combined to obtain the remarkable relation:

$$\gamma = 1 + \frac{\beta}{\alpha} \tag{4.20}$$

so that we see that for $\beta > 0$ and $\alpha > 0$ equation 4.7 gives us a growing neutrino density.
When neutrinos become non-relativistic our model shows a completely different behaviour: with $w_\nu = 0$ the interaction term in equation 4.10 is switched on; the scaling regime ends and the dynamics is described by a different attractor [5], where scalar field and neutrinos become dominant. In this second phase we have [69]:

$$\begin{aligned} \Omega_\phi = 1 - \Omega_\nu &= 1 - \frac{1}{\gamma} + \frac{3}{\alpha^2\gamma^2}, \\ w = \frac{p_\phi}{\rho_\phi + \rho_\nu} &= -1 + \frac{1}{\gamma} \end{aligned} \tag{4.21}$$

where $\Omega_M = \Omega_{cdm} + \Omega_b + \Omega_\nu$ for $t \to \infty$ becomes $\Omega_M \sim \Omega_\nu \sim 1/\gamma$. The present value $\Omega \approx 0.25$ indicates that we're in the middle of a transitin from matter to dark energy domination.

Combining equation 4.10 with the result:

$$\frac{\partial V(\phi)}{\partial \phi} = -\frac{\alpha}{M_p} V(\phi) \tag{4.22}$$

we see that that when $\beta\rho_\nu = -\alpha V(\phi)$ the evolution of the field stops at a value $\phi(t_c) \equiv \phi_c$. Thus, for $t \geq t_c$ we recover the behaviour of the standard ΛCDM model, where the cosmological constant assumes the value of $V(\phi_c)$.

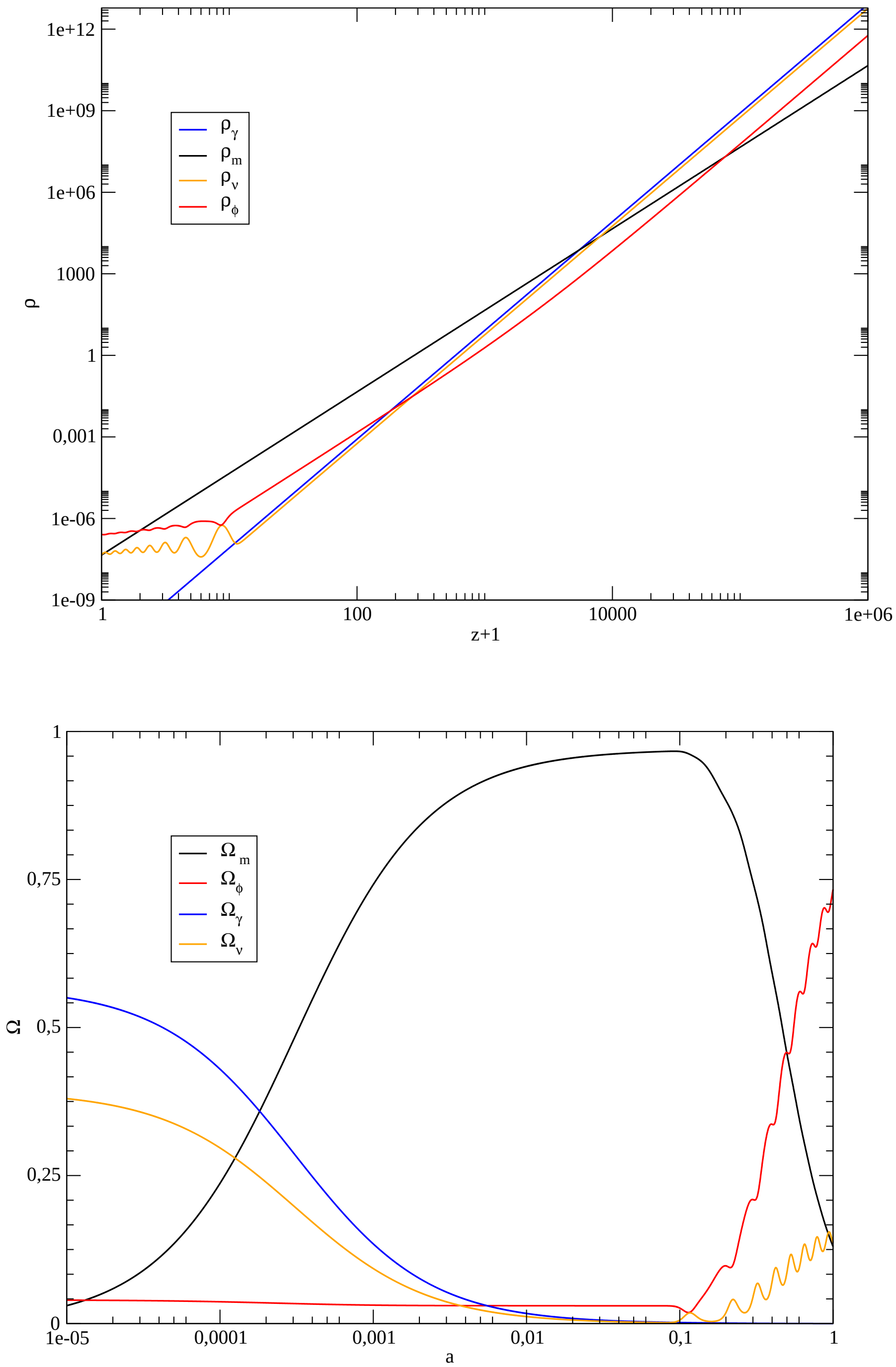

Figure 4.3 — The evolution of background densities and density fractions in a coupled neutrino scenario with $\beta = 50$, $\alpha = 10$ and $\Omega_\nu = 0.01$

4.4.2 Observable Features

The whole evolution of the universe is determined by the value of α and β (which are the most relevant ones in our model) and the value of $m_\nu^{(0)}$ at some given time t_0. From 4.13 we see that the value of α can be constrained by measures on early dark energy coming from SNe Ia and CMB [25]. Furthermore, if we assume that the ratio Ω_ν/Ω_ϕ has currently reached its asymptotic value 4.19 we have:

$$\Omega_\phi(t_0) = \left[\frac{\gamma}{1-\frac{3}{\alpha^2\gamma^2}} - 1\right]\frac{m_\nu(t_0)}{30.8h^2 eV} \approx \frac{\gamma m_\nu(t_0)}{16eV} \tag{4.23}$$

which yields, for the present dark energy density, the follwing expression in terms of γ and m_ν:

$$[\rho_\phi(t_0)]^{1/4} = 1.07\left(\frac{\gamma m_\nu(t_0)}{eV}\right)^{(1/4)} 10^{-3}\text{eV}. \tag{4.24}$$

We can also relate the present day equation of state to the neutrino mass using the previous result and 4.19, obtaining the remarkable expression:

$$w = -1 + \frac{m_\nu(t_0)}{12eV} \tag{4.25}$$

which, for example, gives $m_\nu(t_0) < 2.4eV$ for $w < -0.8$.

4.5 Linear Perturbations

After having determined some interesting results on background quantities, we'll now discuss some important results related to the resolution of the first order perturbation theory[1] for the coupled fluid of neutrinos and dark energy.

4.5.1 Evolution Equations in the Newtonian Gauge

In the growing neutrino scenario, we can write the evolution equations for the density contrasts in the Newtonian gauge (see appendix D) as [58]:

$$\delta'_\phi = 3\mathcal{H}(w_\phi - c_\phi^2)\delta_\phi - \beta(\phi)\phi'\frac{\rho_\nu}{\rho_\phi}[(1-3w_\nu)\delta_\phi - (1-3c_\nu^2)\delta_\nu]$$

[1] For a more in-depth analysis of the perturbation theory we refer to the work of Ma and Bertschinger [54] while many basic results on the perturbed Boltzmann equation can be found in [21]

$$-(1+w_\phi)(kv_\phi)(k\nu_\phi+3\Phi')$$
$$+\frac{\rho_\nu}{\rho_\phi}(1-3w_\nu)\left(\beta(\phi)\delta'+\frac{d\beta(\phi)}{d\phi}\phi'\delta\phi\right) \tag{4.26}$$

$$\begin{aligned}\delta'_\nu &= 3(\mathcal{H}-\beta(\phi)\phi')(w_\nu-c_\nu^2)\delta_\nu-(1+w_\nu)(kv_\nu+3\Phi')\\ &\quad -\beta(\phi)(1-3w_\nu)\delta\phi'-\frac{d\beta(\phi)}{d\phi}\phi'\delta\phi(1-3w_\nu).\end{aligned} \tag{4.27}$$

The δs, called density contrasts, are defined as:

$$\delta_f=\frac{\delta\rho_f}{\bar{\rho}_f} \tag{4.28}$$

where the $\delta\rho_f$ is the over/under density of the fluid f with respect to the average background density $\bar{\rho}_f$.

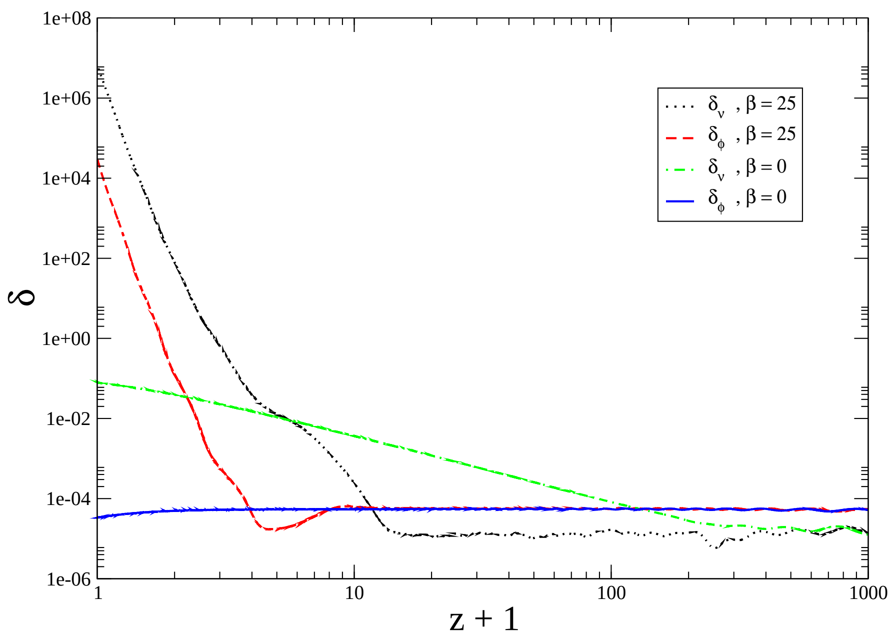

Figure 4.4 — Evolution of density contrasts in coupled and uncoupled quintessence models: note the enhancement of both scalar field and neutrino perturbations caused by the coupling.

Velocity perturbations, which appear into the evolution equations for the density contrasts, evolve according to:

$$\begin{aligned} v'_\phi &= -\mathcal{H}(1-3w_\phi)v_\phi - \beta(\phi)\phi'(1-3w_\nu)\frac{\rho_\nu}{\rho_\phi}v_\phi - \frac{w'_\phi}{1+w_\phi}v_\phi + kc_\phi^2\frac{\delta_\phi}{1+w_\phi} \\ &+k\Psi - \frac{2}{3}\frac{w_\phi}{1+w_\phi}k\pi_{T_\phi} + k\beta(\phi)\delta\phi\frac{\rho_\nu}{\rho_\phi}\frac{1-3w_\nu}{1+w_\phi}, \end{aligned} \tag{4.29}$$

$$\begin{aligned} v'_\nu &= (1-3w_\nu)(\beta(\phi)\phi' - \mathcal{H})v_\nu - \frac{w'_\nu}{1+w_\nu}v_\nu + kc_\nu^2\frac{\delta_\nu}{1+w_\nu} \\ &+k\Psi - \frac{2}{3}k\frac{w_\nu}{1+w_\nu}\pi_{T_\nu} - k\beta(\phi)\delta\phi\frac{1-3w_\nu}{1+w_\nu}. \end{aligned} \tag{4.30}$$

We also define the gravitational potentials Φ and Ψ as:

$$\Phi = \frac{a^2}{2k^2M^2}\left[\sum_\alpha(\delta\rho_\alpha + 3\frac{\mathcal{H}}{k}\rho_\alpha(1+w_\alpha v_\alpha))\right] \tag{4.31}$$

$$\Psi = -\Phi - \frac{a^2}{k^2M^2}\sum_\alpha w_\alpha\rho_\alpha\pi_{T_\alpha} \tag{4.32}$$

where π_{T_α} is the anisotropic stress for the species α.

If we solve the perturbed Klein-Gordon equation (see [58]) we obtain the expression for the linear perturbations of the scalar field:

$$\delta\phi = \frac{\phi' v_\phi}{k}, \tag{4.33}$$

$$\delta\phi' = \frac{\phi' v'_\phi}{k} + \frac{1}{k}\left[-2\mathcal{H}\phi' - a^2\frac{dU}{d\phi} + a^2\beta(\phi)(\rho_\nu - 3p_\nu)\right]v_\phi \tag{4.34}$$

4.5.2 The Perturbed Boltzmann Equation

In order to be able to compute the evolution of neutrinos in the presence of a coupling with the quintessence scalar field, we recall that pressure and energy density are determined by the relations:

$$\rho_\nu = a^{-4}\int q^2 dq d\Omega \epsilon(\phi) f(\vec{x}, q, \tau, \hat{n}) \tag{4.35}$$

$$p_\nu = \frac{a-4}{3}\int q^2 dq d\Omega \frac{q^2}{\epsilon(\phi)} f(\vec{x}, q, \tau, \hat{n}) \tag{4.36}$$

where we write the neutrino distribution function f as:

$$f(\vec{x},\tau,q,\hat{n}) = f_0(q)[1+\Psi_{ps}(\vec{x},\tau,q,\hat{n})]. \tag{4.37}$$

In the above equations we have defined the term $f_0(q)$ as the zeroth-order neutrino distribution (i.e. a Fermi-Dirac one), q as the comoving 3-momentum, $\vec{x}$ as the spatial coordinate, τ as the conformal time and $\hat{n}$ as the versor of the direction of observation.

To solve 4.35, we therefore need to find the form of the perturbed distribution function Ψ_{ps}, solving the Boltzmann equations for coupled neutrinos (see for example [54], [47]). This equation, in its most general form, is simply:

$$\frac{Df}{d\tau} = \frac{\partial f}{\partial \tau} + \frac{\partial \vec{x}}{\partial \tau}\frac{\partial f}{\partial \vec{x}} + \frac{\partial q}{\partial \tau}\frac{\partial f}{\partial q} + \frac{\partial \hat{n}}{\partial \tau}\frac{\partial f}{\partial \hat{n}} = C[f] \tag{4.38}$$

where the right hand involves all terms due to collisions. Interactions and perturbations of the metric (see appendix D) have to be considered when expanding this equation for the coupled neutrinos; it can be therefore shown that the Boltzmann equation for the perturbed neutrino distribution in the Fourier space and in the newtonian gauge takes the form [71], [54], [47]:

$$\begin{aligned}
\frac{\partial \Psi_{ps}}{\partial \tau} &+ i\frac{q}{\epsilon}(\vec{n}\cdot\vec{k})\Psi_{ps} + \frac{d\ln f_0}{d\ln q}\left[-\Phi' - i\frac{\epsilon}{q}(\vec{n}\cdot\vec{k})\Psi\right] = \\
&= i\frac{q}{\epsilon}(\vec{n}\cdot\vec{k})k\frac{a^2 m_\nu^2}{q^2}\frac{\partial \ln m_\nu}{\partial \phi}\frac{d\ln f_0}{d\ln q}\delta\phi
\end{aligned} \tag{4.39}$$

which can be solved expanding Ψ_{ps} in a Legendre series:

$$\Psi_{ps}(\vec{k},\tau,q,\hat{n}) = \sum_{l=0}^{\infty}(-i)^l(2l+1)\Psi_{(ps)l}(\vec{k},q,\tau)P_l(\vec{k}\cdot\hat{n}) \tag{4.40}$$

We can write explicitly the Boltzmann hierarchy for neutrinos:

$$\begin{aligned}
\Psi'_{ps,0} &= -\frac{qk}{\epsilon}\Psi_{ps,1} + \Phi'\frac{d\ln f_0}{d\ln q} \\
\Psi'_{ps,1} &= \frac{qk}{3\epsilon}(\Psi_{ps,0} - 2\Psi_{ps,2}) - \frac{\epsilon k}{3q}\Psi\frac{d\ln f_0}{d\ln q} + \kappa, \\
&\dots \\
\Psi'_{ps,l} &= \frac{qk}{2l+1}\left[l\Psi_{ps,l-1} - (l+1)\Psi_{ps,l+1}\right], \quad \forall l \geq 2.
\end{aligned} \tag{4.41}$$

where:

$$\kappa = -\frac{1}{3}\frac{q}{\epsilon}k\frac{a^2 m_\nu^2}{q^2}\frac{\partial \ln m_\nu}{\partial \phi}\frac{d \ln f_0}{d \ln q}\delta\phi. \tag{4.42}$$

With these expressions, from 4.35 we can calculate the perturbed energy density and pressure for the neutrinos:

$$\delta\rho_\nu = a^{-4}\int q^2 f_0(q)\left[\epsilon(\phi)\Psi_{ps,0} + \frac{\partial\epsilon(\phi)}{\partial\phi}\delta\phi\right] d\phi d\Omega \tag{4.43}$$

$$\delta p_\nu = \frac{a^{-4}}{3}\int \frac{q^4}{\epsilon^2(\phi)} f_0(q)\left[\epsilon(\phi)\Psi_{ps,0} - \frac{\partial\epsilon(\phi)}{\partial\phi}\delta\phi\right] d\phi d\Omega \tag{4.44}$$

4.5.3 Neutrino Clustering

As we have seen in the previous sections, a coupling between neutrinos and scalar field dark energy induce important changes in our evolution equations for density perturbations, with dramatic result with respect to the growth of the perturbations, a feature shared by most of the coupled dark energy models [7]. Therefore, having seen the effect of neutrino masses alone on matter power spectra (figure 4.1), we shall expect some stronger signatures of neutrino interaction in the dark sector in galaxy clustering [58], [61].

For $m_\nu \leq 2$eV we expect neutrinos to become non relativistic at $z_R \approx 5$, so that for $z > z_R$ neutrinos have been free-streaming suppressing perturbations' growth inside the horizion. On the other hand, larger fluctuations are still present and start to grow with a large growth rate for $z < z_R$, opening the possibility for neutrinos to form lumps [14] on supercluster scales; thus providing an observable effect of growing neutrino scenario. In fact, while neutrinos grow non linear at a redshift $z \approx 1$, forcing us to abandon linear perturbation theory, the formation of structures on supercluster scales (mediated either by gravity or by the scalar field) is still an open question that requires the solution of hydrodinamical equations for a spherically symmetric neutrino overdensity [73]. Nonetheless, the linear approximation gives us valuable hints and quantitative limits on the late-time behaviour of the model.

We can distinguish four separate regimes based on the different rate of perturbations' growth within different cosmological scales, namely:

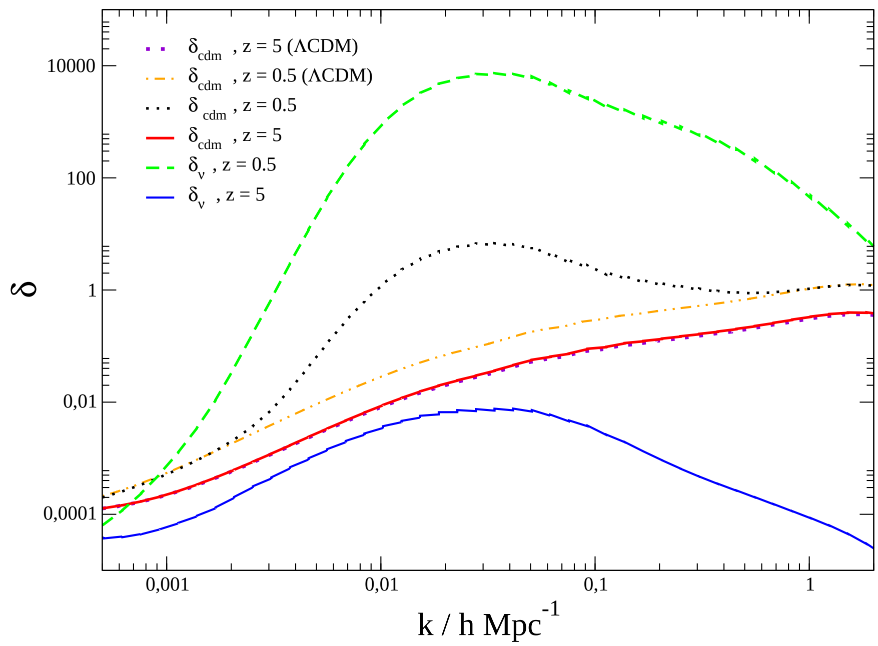

Figure 4.5 — Longitudinal density perturbations for both CDM and neutrinos vs wavenumber k in the linear approximation. We also show the results for CDM fluctuations for a reference ΛCDM at $z = 0.5$ and $z = 5$.

(a) On larger than superclusters scales the universe is still homogeneous and perturbations are still linear today

(b) On supercluster scales (from 14.5 Mpc to approximately 4.4×10^{-3}) strong nonlinearities, enhanced by the coupling with quintessence, forming potential wells where both scalar field and CDM could fall into. This effect also induces CDM to cluster earlier with respect to the concordance ΛCDM model.

(c) On lenghts included between 0.9 Mpc and 14.5 Mpc we expect CDM to take over since neutrinos approach their free-streaming scale, under which perturbations are washed out.

(d) On very small scales, below clusters, CDM becomes highly nonlinear, while neutrinos enter the free streaming regime.

Observations

One may ask about the observable consequences of this model on supercluster scales, where we expect neutrino clustering to take the lead.
In fact, such an effect is supposed to leave an imprint on CMB-fluctuations, in particular through the integrated Sachs-Wolfe (ISW) effect. In dealing with this latter phenomena, however, we must take great care in handling nonlinear contributions, which should reduce by several orders of magnitude the overall contribution of the ISW to the large-scale CMB perturbation. Indeed, as shown in fig. 4.4, perturbation theory (which is based on the assumption of a small δ) must break down at $z \approx 3$, when δ_ν is ~ 1, and it won't be reliable on smaller redshifts, where δ_ν eventually grows to 10^6. However, a more in-depth analysis of this effect will be carried on in chapter 6, where we'll try to constrain the free parameters of the model using WMAP 5 years data.

A second possibility concerns the detection of structures on very large scales, which could be found via their gravitational potential. In fact, these structures could not form by gravitational means alone, but require additional interactions (provided, in our model, by quintessential scalar field) which are obviously absent in the ΛCDM concordance model. Therefore, their detection would be a clear hint for physics beyond the cosmological standard model.

Chapter 5

Parameter Constraint from Supernovae

As we have seen in the previous section, coupled neutrino models are characterized by a great number of significant phenomenological features, which can be used to constrain strongly the possible values of its two free parameters.

Remarkably, as a first step, we could gather some important information just looking at the non-perturbative aspects of the cosmological evolution, i.e., how the different components of the universe evolve throughout the different cosmological epochs: this behaviour is strongly correlated to the quintessence's coupling to neutrinos (which determines the entrance into the dark energy-dominated era) and to the quintessence's potential (which constraints the amount of early dark energy).

5.1 Analysis Techniques

Before entering into the details of the results, we'll briefly outline both the technique used and the assumptions that have been made throughout this first part of our work.

The whole analysis was carried using a modified version of the publicly available Boltzmann-code CMBEASY (see Appendix A.1) which allowed us to calculate the background evolution in the presence of a neutrino-quintessence coupling.

The constraining procedure is then based on a Markov Chain Monte Carlo (see Appendix A.4) analysis, which enables us to obtain the confidence intervals and likelihoods of the different parameters through direct comparison with a set of experimental data. This entire MCMC analysis was based on the cosmological constraint packet *Analyze This!*, an extension of the CMBEASY code.

5.1.1 The Riess Gold Sample

SNe Ia light curves measurements are among the most valuable ones to study and constrain properties of dynamical dark energy [51]. The dataset that we have used for comparison is the so called Riess "gold" sample [33], a collection of 182 high-redshift ($z > 1$) Ia type supernovae detected with the Hubble space telescope from 2004 to 2006. This sample confirms (at 98% confidence level) the transition from a decelerated to an accelerated expansion at a redshift of $z \sim 1$, confirms the presence of a cosmological constant-type fluid ($w = -1$) and rules out rapidly-changing dark energy models ($\frac{dw}{dz} >> 1$).

5.2 Preliminary Considerations

Before actually running the chains, we had to deal with some matters, namely:

- choosing a set of MC parameters
- choosing a suitable interval for every free parameter of our MC run
- avoiding computation of unphysical models
- improve computational speed

Monte Carlo Parameters

We chose to run our Monte Carlo Markov Chain with six free parameters, namely: Ω_{CDM}, Ω_b, h (the Hubble constant measured in units of $100\frac{km}{sMpc}$), Ω_ν, α and β. The latter three are the free parameters of our model, i.e. the neutrino density (which is related to the yet unknown total neutrino mass), the exponential potential α and the coupling β. Since we assume a flat universe, the dark energy density is simply given by: $\Omega_\phi = 1 - \Omega_{CDM} - \Omega_b - \Omega_\nu - \Omega_\gamma$.

In addition to the three unknown parameters, in our MCMC we have included Hubble's constant and the total matter fraction (the sum of Ω_{CDM} and Ω_b), which in our model could have differen best-fit values than ΛCDM.

Interval Selection

After having selected a suitable set of parameters, we had to correspondingly impose boundaries on them. For the Ωs and the Hubble constant our choices were straightforward, as we simply loosened usual ΛCDM parameter intervals, which we expect not to be too different in our model.

On the other hand, we had to deal with two model parameters whose values were *a priori* completely unknown. As far as α is concerned, the lower bound was chosen on the following grounds:

Radiation Attractor: we implemented an algorithm which initialized ϕ directly on the radiation attractor, using the formula:

$$\phi_0 = \frac{M_p}{\alpha} \ln \frac{4}{3\alpha^2} \frac{\Omega_\nu^0 + \Omega_\gamma^0}{1 - \frac{4}{\alpha^2}}$$

Although this choice corresponds to a fine-tuning of the scalar field, it can be safely implemented without dramatic influences on the physics of the model. In fact, we could have chosen to pick-up a random value (within an interval of, let's say, 1 to 10 Planck masses) to initialize ϕ; but this would have forced us to implement also a "trigger" algorithm, to discard unphysical early dark energy dominated solutions, which can take place for some particular initial values. But since late-time physics effects will be the same for most of the ϕ_0s, we can safely fine tune ϕ to avoid random picking and triggering algorithms saving valuable computational time. Therefore, the expression for the field to be on the radiation attractor implies $\alpha > 2$.

Early Dark Energy: since on the radiation attractor we have $\Omega_\phi = \frac{\Omega_\gamma + \Omega_\nu}{\alpha^2}$, early dark energy constraints from BBN impose on α similar lower bouds.

In the end, we found appropriate to constrain α between 5 (which is almost the lower value possible) and 50, which we considered to be reasonably high.

In the case of the coupling parameter β, we only knew it had to be greater than zero, since $\beta = 0$ would correspond to the uncoupled case without late time acceleration. Therefore we set to zero the lower bound, expecting a lower value $\beta_{min} > 0$ to arise naturally from the MCMC. On the other hand, since theoretical considerations alone couldn't limit the upper value of our β, we based our choice of the higher extreme of the interval on the numerical simulations of the background, which showed good results (i.e. Ω_ϕ domination for $z \geq 0.5$) for $\beta \sim 50 - 100$.

5.3 Monte Carlo Run Results

5.3.1 First Run

On the grounds of our previous considerations, for our first run we have chosen the following parameters and intervals, with a flat prior:

MC Parameter	Lower Bound	Higher Bound	Initial Step Size
Ω_ν	0.01	0.1	0.01
Ω_{CDM}	0.1	0.4	0.1
Ω_b	0.01	0.1	0.01
h	0.5	0.85	0.1
α	5	50	2
β	0	100	5

Table 5.1 — List of parameters with corresponding intervals and step sizes for the first SNe Ia MCMC run

Then we started two chains and we let them run until $\sim 10,000$ points in the chain were accepted. The two chains were running in a LAM/MPI environment using CPUs from the cosmology cluster of the *Institut fuer Theoretische Physik* in Heidelberg, for a total computing time of around 40 hours. The analysis of the output (including the plot of likelihood intervals) was carried out using the CMBEASY graphical user interface and the *Analyze This!* package (see appendix A.4).

Analysis of the Results

In figure 5.1 we show the marginalized likelihood function for our model's parameter m_ν^{TOT}, α and β, where the bayesian confidence levels at 68%, 95% and 98% are marked by the three differently coloured bins. The three plots in fig. 5.2 show the likelihood contours in the β-α, β-Ω_ϕ and α-Ω_ϕ planes. We explicitly show in table 5.2 our parameter's most likely values together with the related confidence intervals.

Parameter	Maximum Likelihood	68% C.L.	95% C.L.
Ω_ν	0.126	+0.088 -0.052	+0.167 -0.086
Ω_{CDM}	0.182	+0.067 -0.082	+0.116 -0.172
Ω_b	0.073	+0.054 -0.056	< 0.184
Ω_ϕ	0.577	+0.052 -0.053	+0.081 -0.072
Σm_ν (eV)	1.38	+1.28 -1.04	< 4.17
α	12.8	+11.61 -6.7	< 39.98
β	99.99	> 64.37	> 35.33

Table 5.2 — Maximum likelihood and confidence levels for the values of the parameters of the first MCMC SNe Ia run.

From these results, in particular, we can gather important information about the unknown parameters α, β and m_ν^{TOT}. About this latter, our model predicts that a total neutrino mass of

$$m_\nu^{TOT} = 1.38^{+1.28}_{-1.04}$$

should be observed today; a value which is in good agreement with present day earth based experiments on β decay [36], [34], [37] that give:

$$m_\nu < 2.2\text{eV}$$

for a single degenerate neutrino mass. Cosmological constraints would not apply here, since most of them (such as CMB anisotropy and Lyman α measures) refer to the neutrino mass at earlier times, when we assume it to be much smaller than today due to a negligible coupling with the dark energy.

Then we have the β, the coupling between neutrino and scalar field. Its likelihood curve (see fig. 5.1) has a lower bound at $\beta \sim 8$, as expected; while it is not limited from above. This latter phenomenon can be also seen in fig. 5.2, where we notice that the late time dark energy density is substantially independent (above a certain threshold $\beta \sim 30$) from the value of the coupling β.

On the other hand, α's likelihood curve shows upper and lower bounds, substantially constraining this parameter between 5 and 40, with a clear peak in the region $\alpha \simeq 12$. We can also see a loose relation between Ω_ϕ, with higher dark energy density fractions more likely to be present with smaller coupling.

For completeness, in table 5.3 we show the values of the best fit model, i.e. the model with the overall highest likelihood.

Parameter	Best Fit Value
Ω_ν	0.156
Ω_{CDM}	0.288
Ω_b	0.049
Ω_ϕ	0.506
α	26.35
β	86.49

Table 5.3 — Best fit model as obtained from the SNe Ia Riess gold dataset first MCMC run.

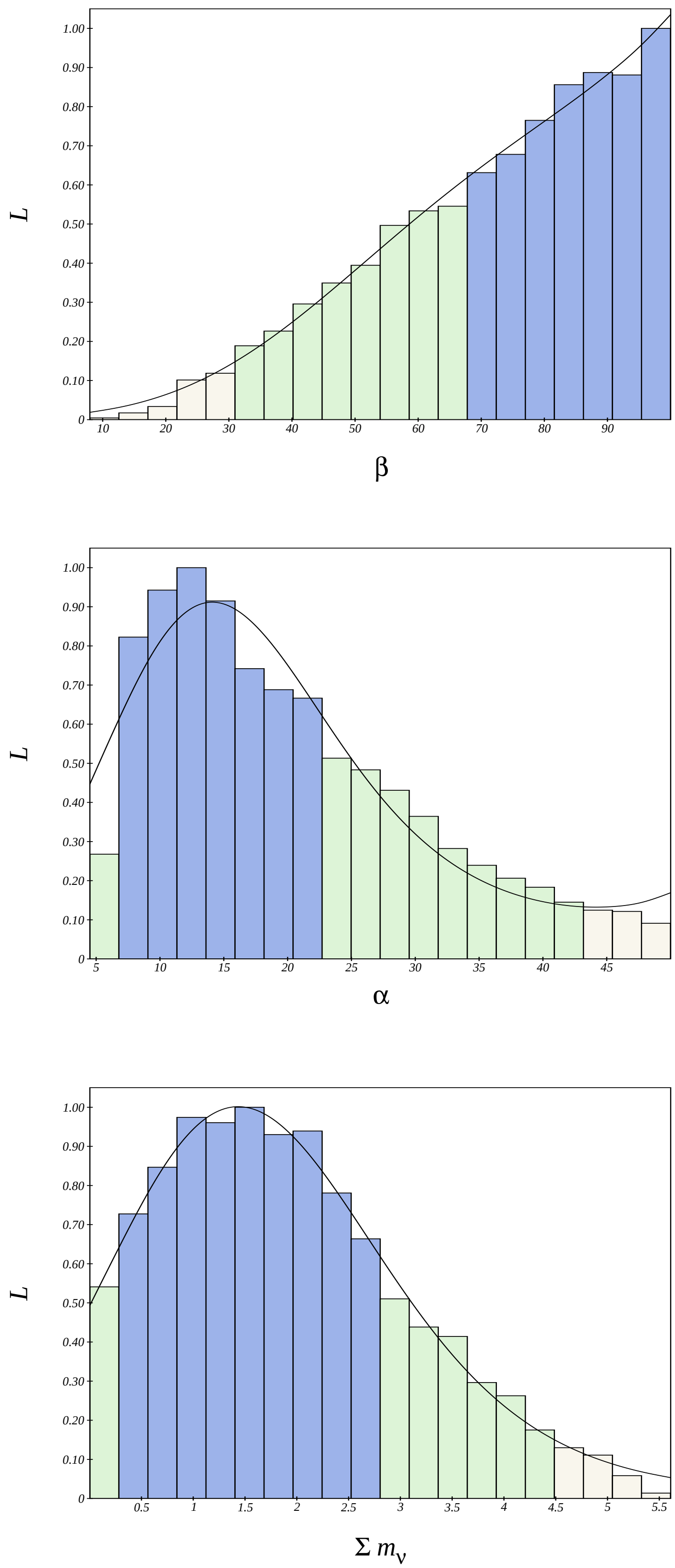

Figure 5.1 — Likelihood curves for, β, α and m_ν^{TOT} obtained in the first MCMC SNeIa run. Every plot is made marginalizing over all the other parameters.

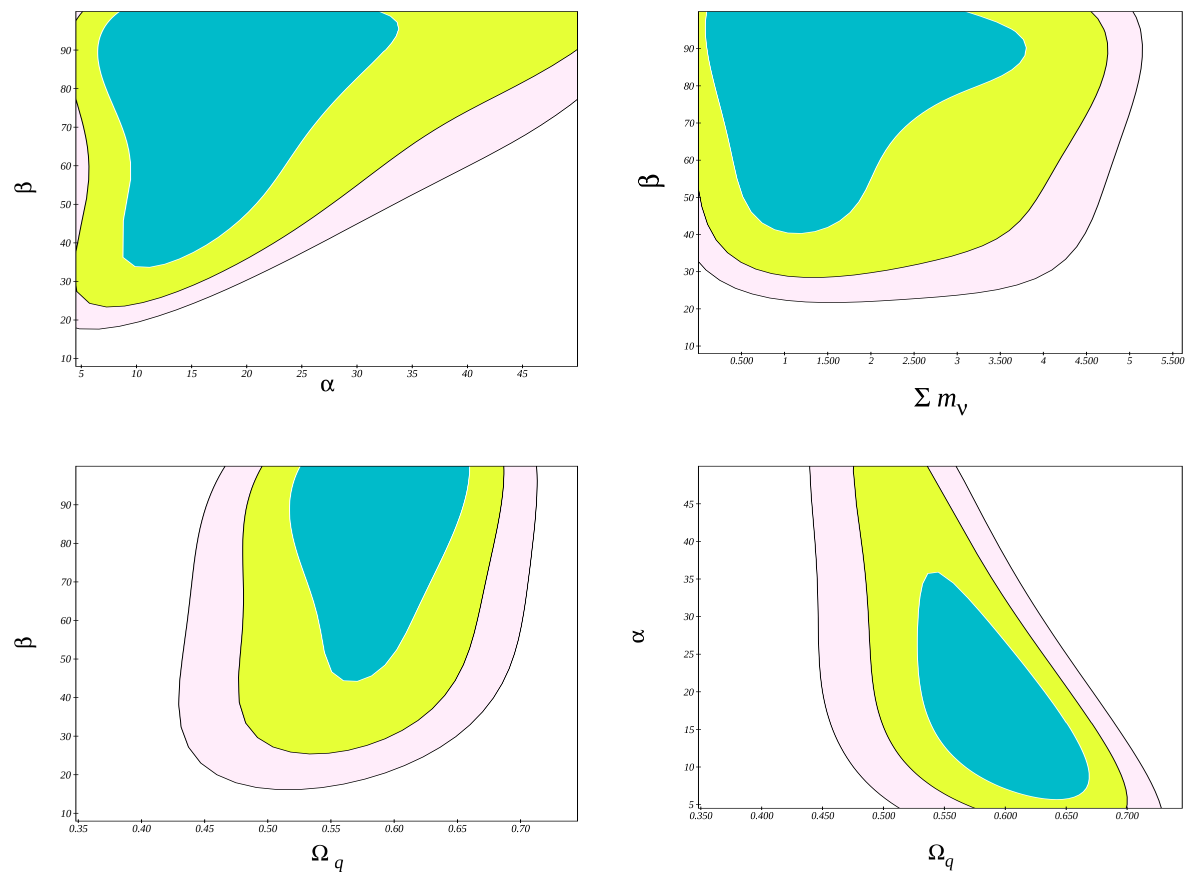

Figure 5.2 — Confidence intervals for $\alpha - \beta$, $\beta - m_\nu$, $\Omega_q - \beta$ and $\Omega_q - \lambda$ obtained in the first MCMC SNeIa run. Differently shaded regions represent the 65%, 95% and 98% confidence levels.

5.3.2 Second Run: the Small-Coupling Region of the Parameter Space

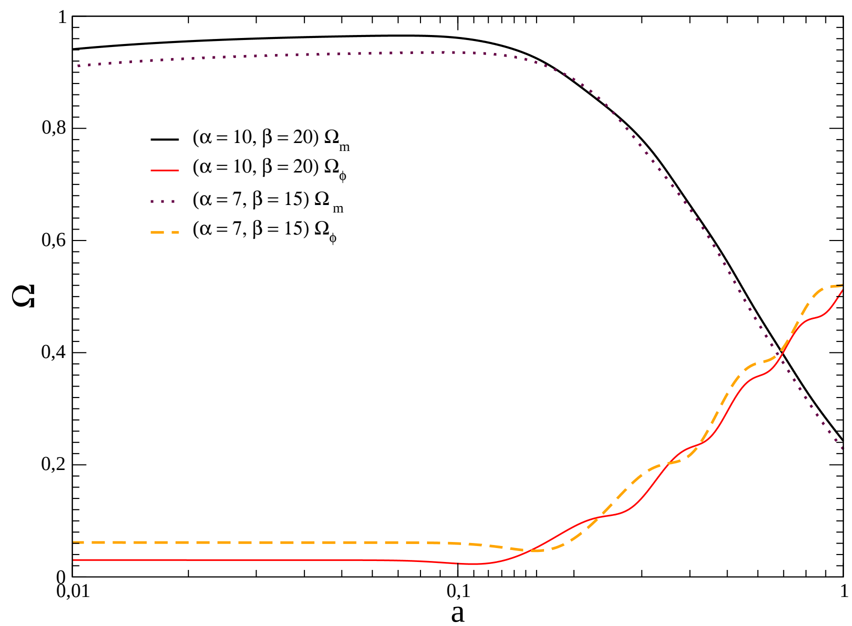

Figure 5.3 — Degeneracy between α and β. A smaller coupling can give rise to the same dark energy density of a bigger one, provided that the potential parameter α is corrispondingly decreased.

A second run has been performed in order to determine whether it was possible to have late time acceleration with a smaller β coupling, using the degeneracy among β, α and m_ν. Given that in our model the quintessence fraction in the scaling regime is given by Ω_ϕ/α^2 we see that the net effect of reducing α is to increase the scalar field's energy density. We also know that, since it is the combined effects of neutrino masses and β that causes the field to stop evolving and start acting like a cosmological constant, an increase in the former may allow a lower value for the latter. Therefore, we have two effects that can compensate a substantial reduction of the coupling parameter. As we will see in the following section, a smaller β is required in order to decrease the size of the ISW, an effect that heavily plagues this kind of model [1]. The latter was the main reason why we wanted to look at

[1]This problem will be deeply analyzed in the next chapter

the shape of the parameter space once tighter constraints on α (which we let run from 5 to 35) and β (going from 0 to 50) are being put, while letting al the other intevals unchanged.

In this second MCMC run we let two chains run for $\sim$ 30 hours until they accepted around 10,000 points each.

Analysis of the Results

Parameter	Maximum Likelihood	68% C.L.	95% C.L.
Ω_ν	0.234	+0.068 -0.055	+0.138 -0.097
Ω_{CDM}	0.167	> 0.099	> 0.055
Ω_b	0.0254	+0.014 -0.014	< 0.05
Ω_ϕ	0.603	+0.041 -0.038	+0.081 -0.072
$\Sigma m_\nu (eV)$	7.28	+1.59 -1.81	+2.41 -2.74
α	11.96	+7.07 -4.49	+13.58 -7.37
β	49.99	> 31.25	> 17.82

Table 5.4 — Maximum likelihood values and confidence levels for parameters of the second MCMC SNe Ia run.

In table 5.4 we show the maximum likelihood and confidence limits on our model's parameters as obtained in our second MCMC run. We see that the biggest effects of our tighter constraints can be seen on Ω_ν and m_ν^{TOT}, which have considerably higher most likely values with respect to our previous run. We stress here that such a high neutrino mass prediction is still consistent, within 2σ, with the earth based experiments we mentioned before which yield an upper limit of 6-7 eV for three almost degenerate neutrinos. This effect is of course a compensation to the reduction of β, as we can see from equation 4.10, which tells us that the onset of the accelerated phase is proportional to $\rho_\nu(1 - w_\phi)\beta$.

A second remarkable feature is the shape of the likelihood curves in the α-β plane (see 5.3.2), where we notice a strong intercourse among the two parameters; in the way we foresaw in the introduction to this paragraph. On the other hand, the contours in the other planes do not show substantial differences to the ones we obtained in our first MCMC run; with an Ω_ϕ almost independent of β above the $\sim$ 20 threshold value and a loose relation with α. In the same way, the marginalized likelihood curve for the scalar field potential's parameter shown in 5.4 has the same peak for $\alpha \sim 12$ we got in our first results.

In table 5.5 we show the best fit model parameter values.

Parameter	Best Fit Value
Ω_ν	0.118
Ω_{CDM}	0.18
Ω_b	0.035
Ω_ϕ	0.675
α	5.16
β	28.98

Table 5.5 — Parameter values for the best fit model from the SNe Ia Riess gold dataset second MCMC run.

In the end, we could see in this second MCMC run that our model can run and reproduce our SNe Ia data with a small er coupling; implying a substantially bigger neutrino mass (and density) which is by no means yet completely ruled out by earth based experiments' bounds. So, after having obtained precious informations on our parameters and on our model's behaviour by looking at the background evolution, we can switch to the study of the perturbative regim e, in particular, we can carry on a detailed analysis of the CMB anisotropy implications of growing mass neutrinos coupled to quintessence.

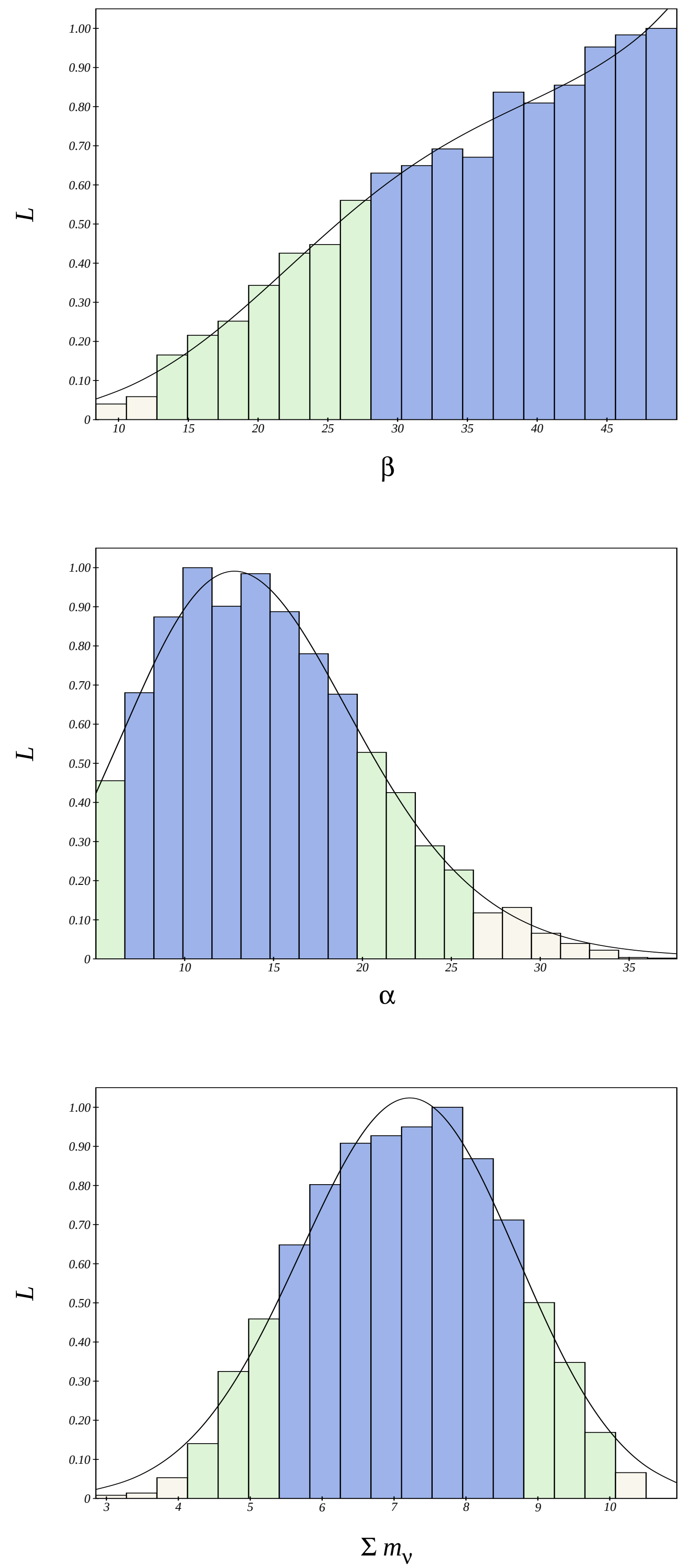

Figure 5.4 — Likelihood curves for m_ν^{TOT}, β and α obtained in the second MCMC SNeIa run marginalizing over all the other parameters.

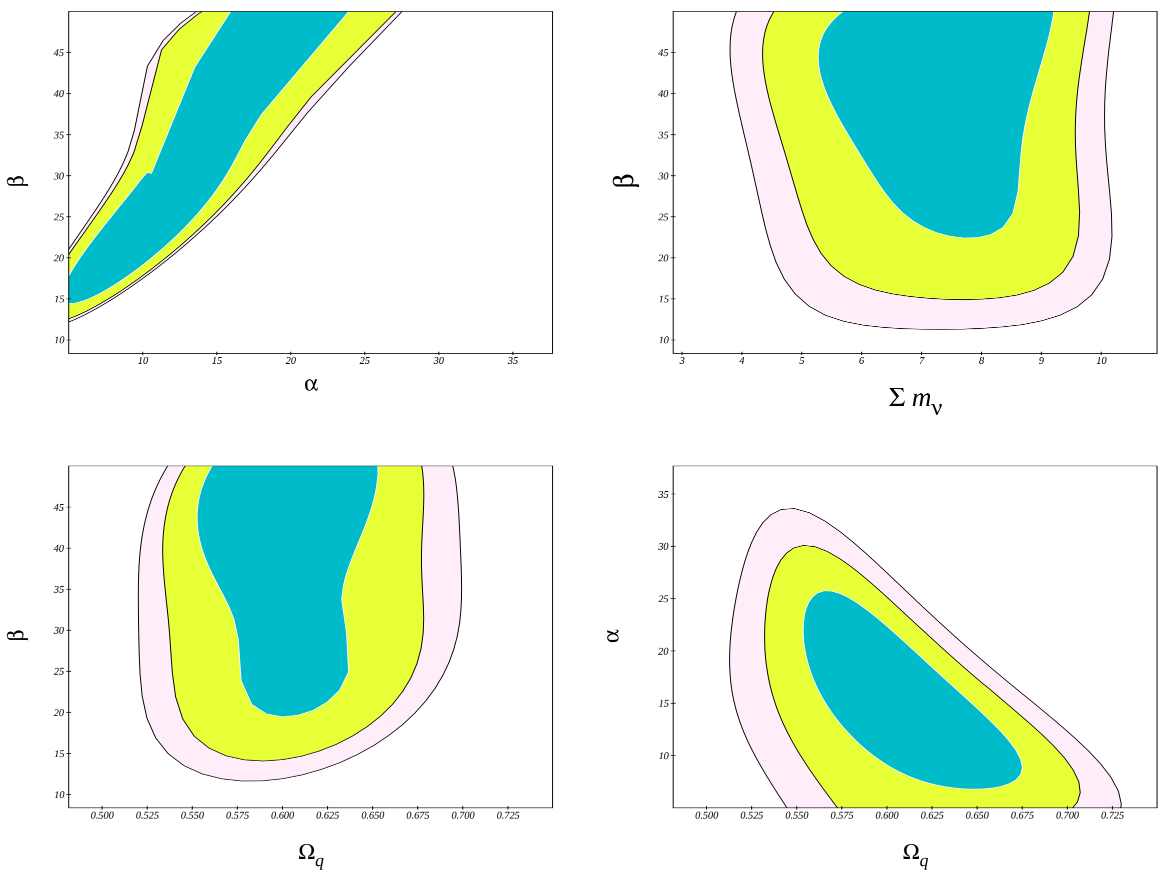

Figure 5.5 — Confidence intervals for α-β, $\beta - m_\nu$, Ω_q-β and Ω_q-λ obtained in the second MCMC SNeIa run. Differently shaded regions represent the 68%, 95% and 98% confidence level.

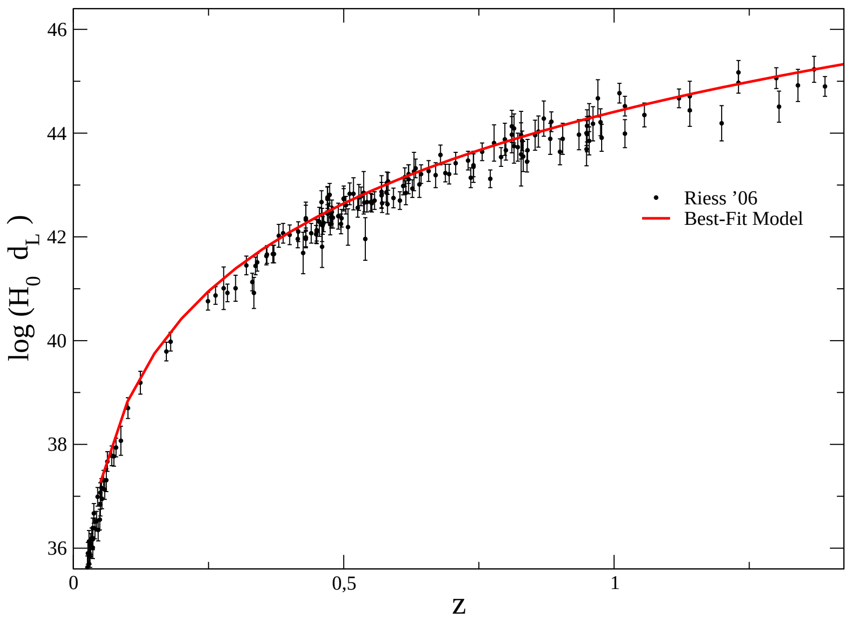

Figure 5.6 — Plot of the best fit model for the second SNe Ia MCMC vs. the Riess 2006 Gold dataset.

Chapter 6

Parameter Constraint from CMB

As we have seen in section 4.2, massive neutrinos have important effects on the outlook of the CMB anisotropy spectrum. Still, these kinds effects can only loosely constrain our model, since we expect that in a growing neutrino model, νs only have a negligible mass during the decoupling era. This feature was stressed before, when explaining why cosmological neutrino mass bouds do not apply in this model.
In fact, the main detectable contributions of our model do not come from the decoupling era but are directly related to the peculiar evolution of neutrino and dark energy densities, that imply important large-scale effects as we will see in the following paragraph.

6.1 The ISW Effect

In section 2.2.2 we mentioned the Sachs-Wolfe effect, which affects by blue (red) shifting photons extiting from under (over) densities at decoupling time. In a similar way, photons entering a potential well are blue (red) shifted if the depth of this well is decreased (increased) when they exit from it; this effect is called integrated Sachs-Wolfe (ISW).
In [28] it is shown that the global contribution to the gauge-invariant multipole spectrum $M(\mu, \tau_0)$ (with τ_0 being the conformal time variable today and $\mu = \frac{\hat{n}\cdot\vec{k}}{|k|}$, $\hat{n}$ being the direction of the photon and $\vec{k}$ the Fourier space vector) takes the form:

$$M(\mu, \tau_0) = \int_0^{t_0} d\tau e^{i\mu k(\tau - \tau_o)} S_T(\tau, k) \tag{6.1}$$

where $S_T(\tau, k)$ is the source term, that can be explicitly written as:

$$\begin{aligned} S_T(\tau, k) &= -e^{i\mu\kappa(\tau)-\kappa(\tau_0)}\left[\dot{\Psi} - \dot{\Phi}\right] + \dot{g}\left[\frac{V_b}{k} + \frac{3}{k^2}\dot{C}\right] \\ &+ \ddot{g}\frac{3}{2k^2}C + g\left[\frac{1}{4}D_g^\gamma + \frac{\dot{V}}{k} - (\Phi - \Psi) + \frac{C}{2} + \frac{3}{2k^2}\ddot{C}\right] \end{aligned} \quad (6.2)$$

In this equation, C is the scattering term entering the photon Boltzmann equation (related to polarization phenomena), D_g^γ is the gauge invariant photon overdensity, V_b is the baryon velocity at decoupling, $\kappa(\tau)$ is the optical depth defined as $\dot{\kappa} = an_e\sigma_T$, $g = \dot{k}exp(\kappa(\tau) - \kappa(\tau_0))$ is the visibility function, Ψ and Φ are the potentials entering the perturbed metric tensor. D_g^γ is the main contribution on scales within the horizion at decoupling time, whereas the term $\Phi - \Psi$, i.e. the Sachs-Wolfe effect, dominates on the largest scales well outside the horizon, inducing perturbations of the form [21]:

$$\frac{\Delta T_k}{T} = -\frac{H_0^2}{2}\frac{\delta_k^{TOT}}{k^2} \quad (6.3)$$

The $\dot{\Phi} - \dot{\Psi}$ in equation 6.2 accounts for the ISW effect, that can be directly related to temperature anisotropies through the formula [15]:

$$\frac{\Delta T}{T} = -\frac{2}{c^2}\int_0^{t_L} [\dot{\Phi}(t) - \Psi\dot{(t)}]dt \quad (6.4)$$

which clearly shows that steep potential derivatives induce huge fluctuations on large scales.

It is now useful to write the explicit form of the longitudinal gravitational potential Φ which depends on the scale k through:

$$\Phi(k) = -\frac{4\pi a^2}{k^2}\left[\delta_{tot} + \frac{3H(1+w)\Theta}{k^2}\right] \quad (6.5)$$

We are then able by the above formulas to relate the evolution of neutrino density contrasts δ_ν discussed in chapter 4.5.3 to the temperature fluctuations observed in the CMB spectrum. We expect the rapid growth of those perturbations to contribute overwhelmingly to the large scale temperature anisotropies, even though, on the other hand, nonlinear effects my dramaticaly affect such an expectation. In the following section we'll introduce a perturbation cutoff, which we will use to model the onset of the regime where first order perturbation theory ceases to be valid.

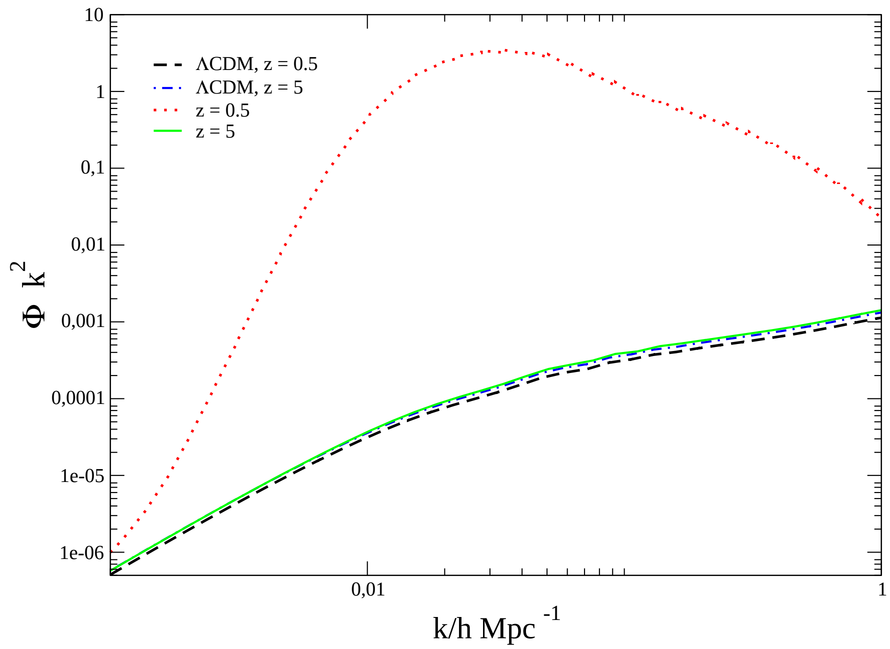

Figure 6.1 — Longitudinal gravitational potential vs wavenumber k at a redshift of $z = 0.5$ and $z = 5$; a reference ΛCDM is also shown.

6.2 The Cutoff

The previous analysis together with the results previously shown in figure 4.4 force us to take into account the strongly nonlinear effects arising from the coupling. Since we do expect perturbation theory to break down at $\delta \sim 1$, our first concern at this stage was to find a suitable stategy to deal with it in order to be able to produce reliable (although approximated) results from Monte Carlo simulations. Our strategy was to introduce a perturbation *cut-off* setting the onset of the nonlinear regime. We assumed that in this latter stage of cosmological evolution clustering effects prevailed on the growth of perturbations, causing neutrinos to decouple from the background evolution. Their contribution to the the overall gravitational potential through equation 6.5 would subsequently be suppressed, and would have to be replaced by the average contribution coming from clustered neutrino lumps [14], [61].

Unfortunately, theory gives us no clear clues on the size and the type of cutoff that we should introduce, since the whole issue of neutrino structure formation hasn't yet been studied in detail enough to provide reliable estimates on the initial conditions which could induce clustering. Therefore, we were left with several viable options when trying to tackle the problem of modelling the transition between the two regimes. Our first guess was to track the evolution of the δs and simply stop them once their value reached unity. However, in this case several questions would arise: should we simply block the evolution of δ_ν once it has reached a value of order one? Or maybe should we stop δ_ν and δ_ϕ at the same time, because of the strong interaction between the two components? How much could we trust the evolution of other δs once we stopped some of them? Rough numerical estimates coulnd't give reliable solutions to these problems.

Therefore, we were elaborated another stategy, facing the problem from a slightly different point of view: instead of looking at the theory to get some kind of reliable cutoff, we decided to use this cutoff as another parameter to be determined by our simulations. Such a cutoff would have to be used in a second step as a boundary condition in the nonlinear hydrodinamycal equations, to see whether this could induce neutrinos to form structures. Since these equations all depend on the gravitational potential through Poisson-type relations (which also include scalar field interaction terms), we chose our cutoff to be a potential cutoff.

In other words, neutrino contributions to the gravitational potential would be stopped once they reached the size of our new parameter $\Delta_c = \Phi_\nu/\Phi_{TOT}$, whose value had to be estimated through our MCMC runs using the WMAP5 data. Again, we stress here that this Δ_c has to be seen as a parameter whose value, at this stage of our knowledge, is *a priori* unknown. What we want to find out is which size Φ_ν can reach in order to induce gravitational and/or scalar field mediated neutrino clustering and preserve at the same time an ISW effect consistent with today's WMAP5 data. What we need to do, then, is to see whether this data-consistent potential may cause neutrino structures to form; an issue that is however out of the scope of this work. We also want to point out that Δ_c doesn't have to be necessarily unity, since it refers only to gravitation: we must keep in mind that in this scenario the strong coupling between νs and ϕ also mediates the clustering, possibly inducing a lower threshold on the Φ that would normally cause neutrino structures to form.

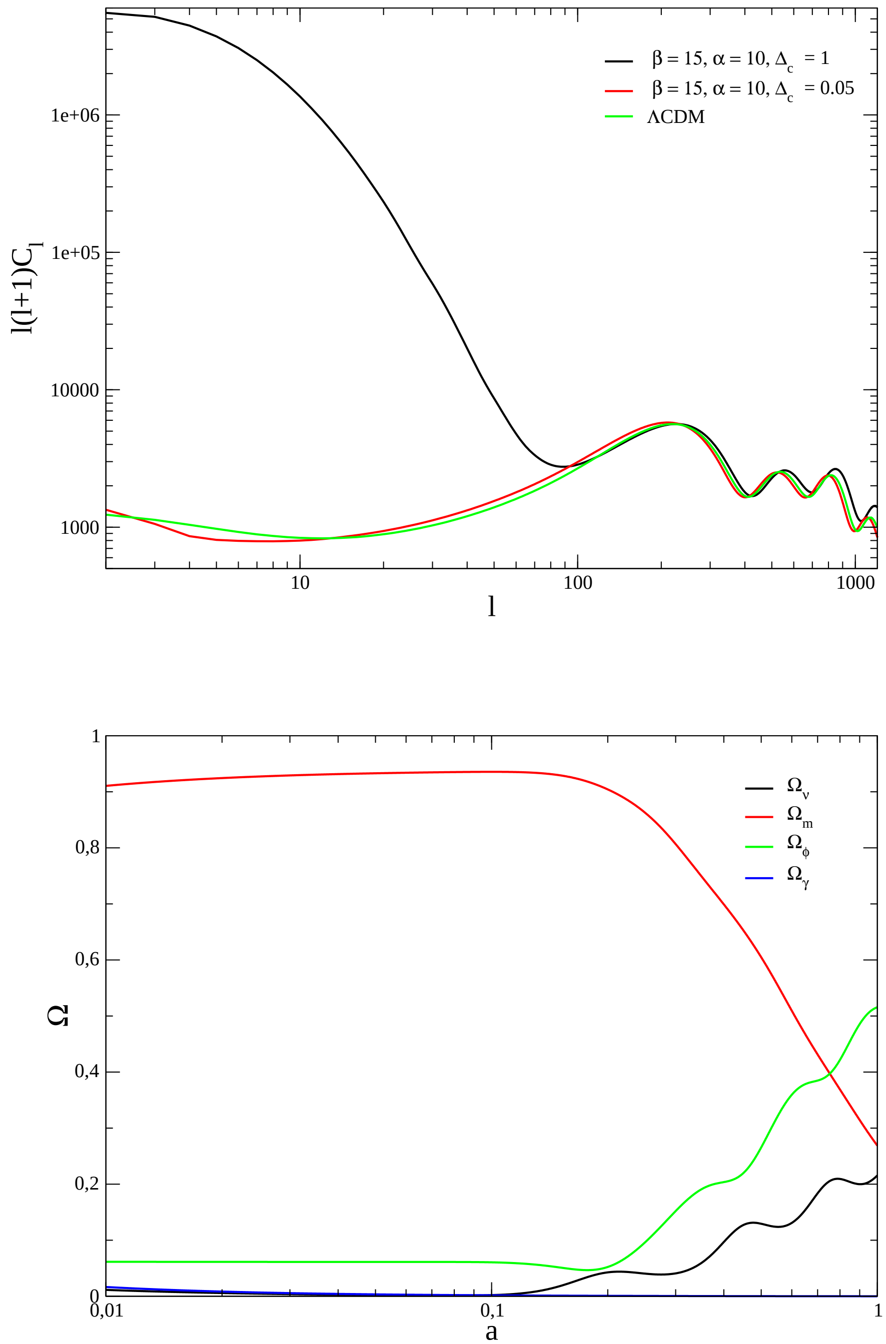

Figure 6.2 — In the first picture we show the CMB anisotropy spectrum for a model with no cutoff (Δ_c=1) and a 5% cutoff. We also print a reference ΛCDM model for comparison. In the second image we also show that this model, with $\beta = 15$ and $\alpha = 10$ can account for the observed late-time accelerated expansion of the universe.

6.3 The WMAP5 Dataset

The Wilkinson Microwave Anisotropy Probe (WMAP) is the first new generation satellite which provided high resolution temperature surveys of the CMB anisotropies, providing full-sky maps with a resolution higher than one degree. WMAP data have been published in 2003 (after the first year of flight), 2005 (WMAP3) and most recently in 2008 (WMAP 5). The latter set, in particular, has been used to put the most stringent neutrino mass limit up to date as well as constraining the main parameters of the standard ΛCDM cosmology [48]. The whole WMAP dataset, together with analysis software, images and results is freely and publicly available on the NASA website [1].

6.4 Preliminary Considerations

In equation 4.27 we see that neutrino density contrasts' evolution in the non-relativistic regime (i.e. when $w_\nu \neq \frac{1}{3}$) is strongly affected by β, as shown also by numerical simulations in figure 6.3, where we also notice that a relatively small change in β modifies the final evolution of δ_ν by several orders of magnitude.

As we have seen before, steep δ derivatives imply also a large ISW, therefore we expect our Δ_c parameter to be strongly correlated with β.

6.4.1 Montecarlo Parameters

In the choice of our MC parameters and intervals, we had to deal with computational time issues. Whereas the computation of the background densities is a matter of a very few seconds, calculating the CMB spectrum requires from 30 to 40 seconds, to which we must add the likelihood computation time. Furthermore, initial testing simulation of this MCMC showed an acceptancy rate of $\sim$ 10%-20%, depending on the number of parameters and the choice of the intervals. If we assume that we need at least $\sim$ 5.000 points to have an efficient exploration of the parameter space, the overall number of models we have to compute goes from 25.000 to 50.000, that is, if we distribute these points among two chains, from four to eight days of computing.

Therefore, to save computing time, we chose a minimum set of MC parameters, i.e. β, α, m_ν and Δ_c, where the former was the only "new" one with respect to the old MCMC runs. We fixed all densities to the most likely

[1] http://map.gsfc.nasa.gov/

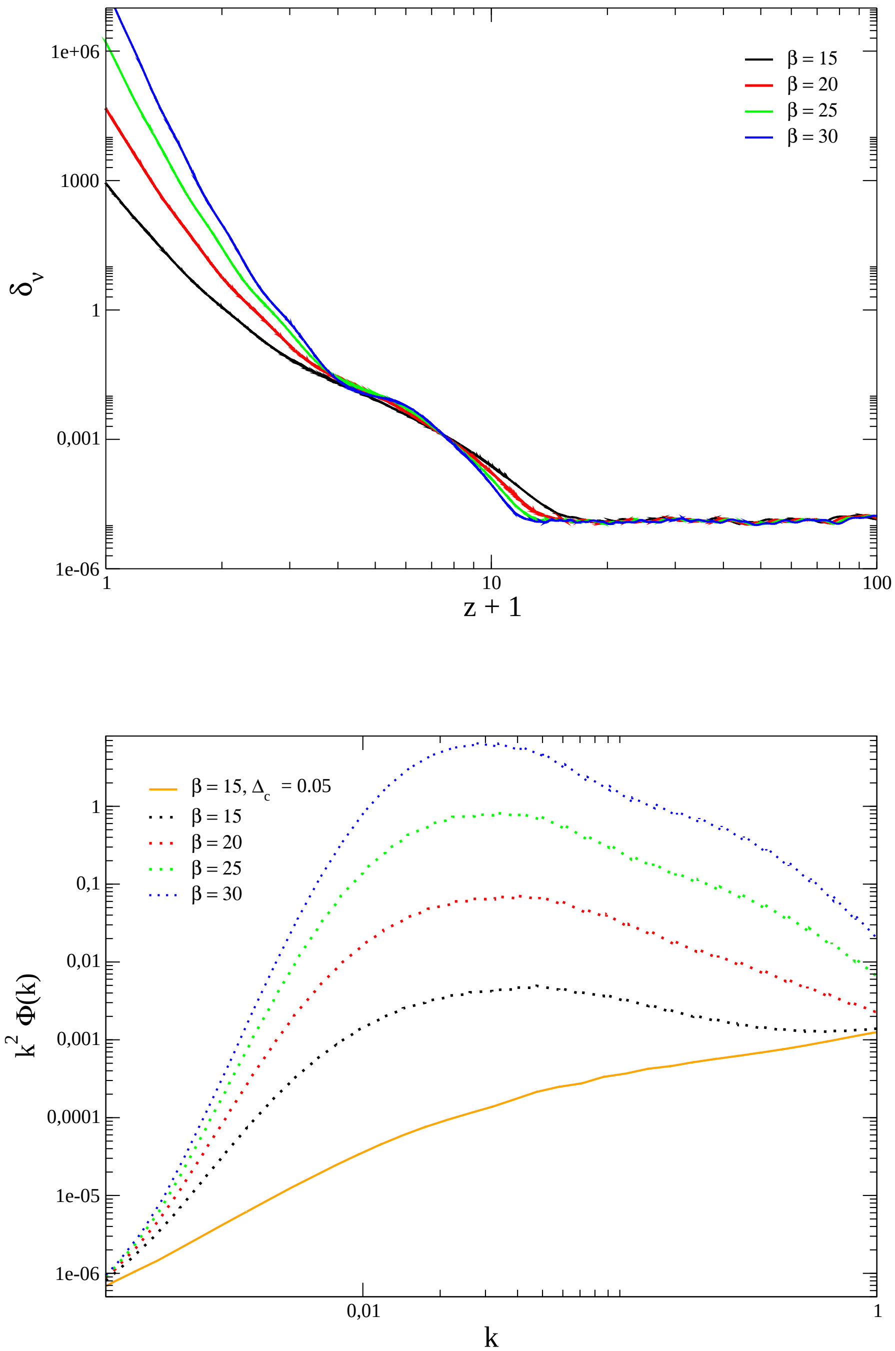

Figure 6.3 — How different βs affect the evolution of the perturbations and of the longitudinal gravitational potentials. We show $\delta_\nu(z)$ and $\Phi(k)$ for $\beta = 15, 20, 25, 30$; in the case of the potentials we also plot a case with $\Delta_c = 0.05$.

values as obtained in the second SNe Ia MC run, with the total density of quintessence determined by the condition of a flat universe. The list of parameter and corresponding intervals are listed in table 6.1:

The intervals were determined on physical grounds. Whereas for our α and

MC Parameter	Lower Bound	Higher Bound	Initial Step Size
Ω_ν	0.01	0.1	0.01
α	5	20	1
β	10	25	1
Δ_c	0.01	1	0.005

Table 6.1 — List of parameters with corresponding intervals and step sizes for the WMAP5 MCMC run.

Ω_ν no particular consideration was required, the strong interplay between β and Δ_c required some additional care. In fact, numerical simulations showed that the CMB spectrum obtained with $\Delta_c < 0.01$, for almost any given β, was equivalent to the $\Delta_c = 0$ case, i.e. where no perturbation growth was allowed. On the other hand, the case with $\beta > 25$ would require $\Delta_c < 0.01$ to produce WMAP 5 consistent CMB spectra. Both these bounds have been implemented in our choice; in addition we put the lowest limit on β to 10 (a relatively high value according to CMB simulations) while we let Δ_c go until 1, i.e., the case in which there's no perturbation cutoff.

Once the intervals and the parameters were chosen, we started two chains and let them run until each one of them acceppted ~ 2.500. The run took approximately one week on a machine running a dual core intel processor.

6.5 Monte Carlo Run Results

The list of the parameters together with the maximum likelihood and the 68% and the 95% confidence level obtained in our runs are shown in table 6.2. In figure 6.4 we show the marginalized likelihood curves for α, β, Δ_c and Σm_ν^{TOT}; while in figure **??** we show the 68%, 95% and 98% confidence level intervals in the planes $\alpha - \beta$, $\alpha - \Delta_c$ and $\beta - \Delta_c$.

These pictures show different constraints than the ones we had in our previous SNe Ia runs. Most notably, the likelihood curve for β has a maximum likelihood value right at the lowest limit of the interval, whereas in the other runs it had exactly the opposite behaviour. However, as we often mentioned in our previous paragraphs, this behaviour was somehow expected; what we

Parameter	Maximum Likelihood	68% C.L.	95% C.L.
Δ_c	0.031	+0.016 -0.016	< 0.066
$\Sigma m_\nu (eV)$	2.25	+0.07 -0.07	+0.14 -0.15
α	14.31	+3.26 -1.28	+5.41 -1.85
β	10.01	< 12.76	< 15.06

Table 6.2 — Maximum likelihood values and confidence levels for parameters of the second MCMC SNe Ia run.

were at most interested in was the tale of this likelihood curve, which could in principle display non trivial superpositions with the one obtained in the SNe Ia.

Another quite remarkable result is the overall size of the cutoff Δ_c, which is peaked around the 0.03 region. Although this might seem an unnaturally low value, we must keep in mind that in our model neutrinos cluster due to the combined effect of gravity and quintessential scalar field interaction: therefore, a small cutoff does not *a priori* rule out our hypothesis of clumping even if the final word on the subject relies on yet to come analytical results.

On the other hand, α is in good agreement with both SNe Ia constraints while m_ν^{TOT} is only consistent with the lower value obtained in the first MC simulation.
In table 6.3 we show for completeness the best-fit values for the four MC parameters of our model.

Parameter	Best Fit Value
m_ν (eV)	2.27
Δ_c	0.052
α	15.05
β	11.36

Table 6.3 — Best Fit Values for the WMAP 5 MCMC

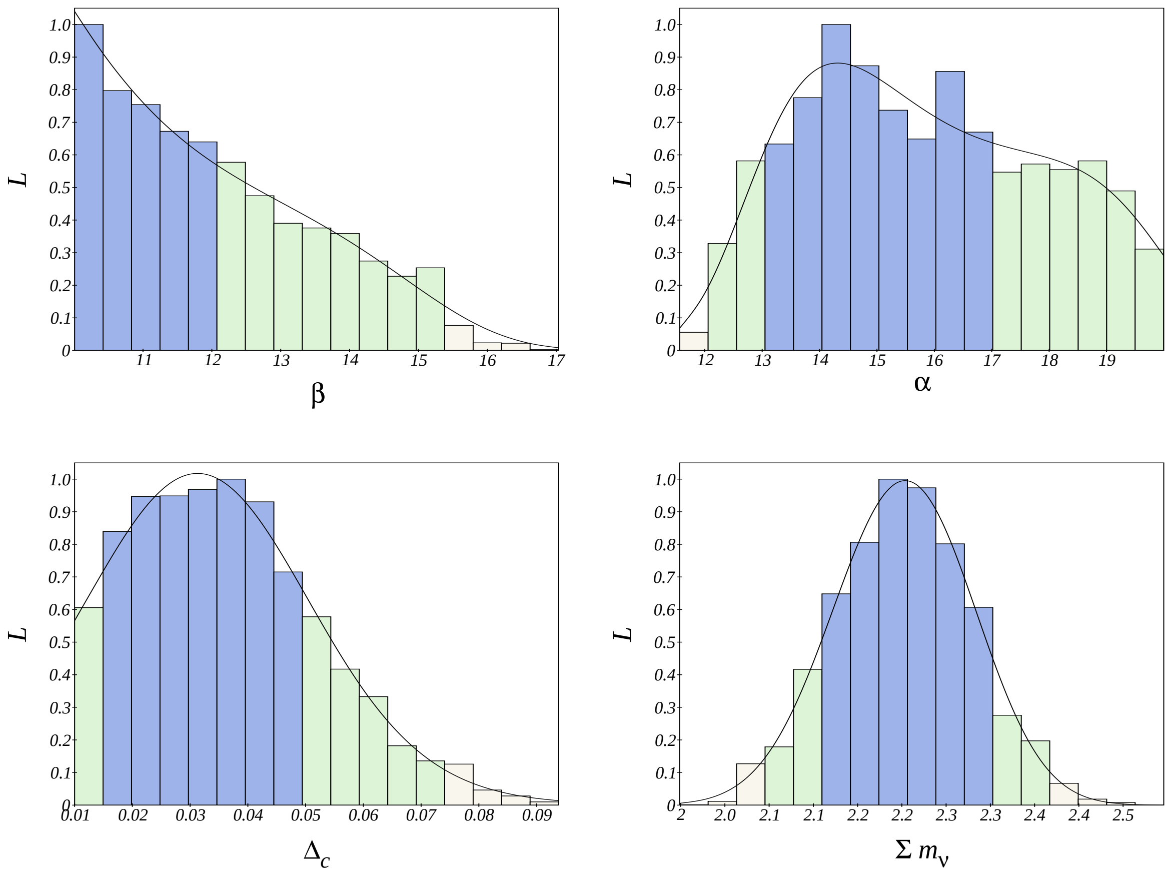

Figure 6.4 — Marginalized likelihood curves for β, α, m_ν^{TOT} Δ_c values obtained from MCMC CMB runs marginalizing over all the other parameters.

Chapter 7

Conclusions

In this work we have performed a broad analysis of a model in which dark energy is coupled to neutrinos, a scenario where νs behave as a non standard form of matter with a growing mass. We also pointed out its main phenomenological and theoretical motivations, namely, the similarity between quintessence and m_ν energy scales and the solution to the main fine-tuning and naturalness problems of the actual cosmological standard model. In fact, it is the entrance into the relativistic regime for massive neutrinos that naturally drives the quintessential scalar field to behave like a cosmological constant, triggering the onset of the accelerated expansion for the universe.

Then, after having written the equations that govern the growth of densities and density perturbations in the coupled neutrino scenario, we have solved them numerically, pointing out some peculiar predictions of our models like the clustering which should take place on very large scales. The following step was to try to constrain the parameters of our model using two kinds of dataset, which we chose to be the Riess Gold SNe Ia sample and the WMAP 5 years collaboration data.

This analysis was carried using the CMBEASY data constraint package *Analyze This!*, which made use of Monte Carlo Markov Chains and the Metropolis algorithm. We performed two different runs of Monte Carlo Markov Chains using SNe Ia data and a single MCMC using WMAP 5 data. Before actually running the chain with the latter dataset, we decided to model nonlinearities taking into account a cutoff, which we used as an additional parameter of our MCMC from which we could gather informations on the maximum size that the neutrino-induced gravitational potential could reach.

We saw then that SNe Ia couldn't provide tight constraints on the value of our coupling parameter β, since late time acceleration requirements were consistent with an arbitrarily high value. On the other hand, WMAP 5 data provided stringent upper limits on this same parameter; at the point that the likelihood curves we obtain from them have a non-zero superposition only at the 3σ confidence level with the second SNe Ia MCMC run. Furthermore, we have seen that the value of the total m_ν, one of the remarkable predictions of our model, depends strongly on the interval we choose for our β; the bigger it is, the smaller should be the neutrino mass.

7.1 Future Developements

The constraints we obtained from SNe Ia and WMAP5 data give us results which are consistent only at the 3σ level, which makes our simple model an unlikely candidate to account for the universe's accelerated expansion. Therefore, we can drop some of the assumptions we made at the beginning, in order to see whether extensions of this model may still provide interesting results.

7.1.1 Out of the Scaling Attractor

We recall here that in our analysis we excluded the interval $\alpha < 5$ since we wanted our model to have an early time scaling regime for quintessence, given by the attractor $\Omega_\phi = \frac{\Omega_\gamma}{\alpha^2}$, which in turn implied that bound due to consistency with BBN limits on early dark energy. However, as is shown in figure 7.1, we see that we can account both for the present CMB anisotropy spectrum and quintessence domination just by dropping this assumption and fine tuning our initial condition to a smaller value for the scalar field ϕ_0.

Even though we would lose an appealing feature of our model, it might be worth in future developements to see whether some combinations of α, β and m_ν admit a broader range of initial field values, removing to some extent the need of fine tuning it. In this way, it is also reasonable to assume that we can find regions of the parameter space where the cutoff Δ_c doesn't have to be as low as the one we found during our WMAP5 based MCMC.

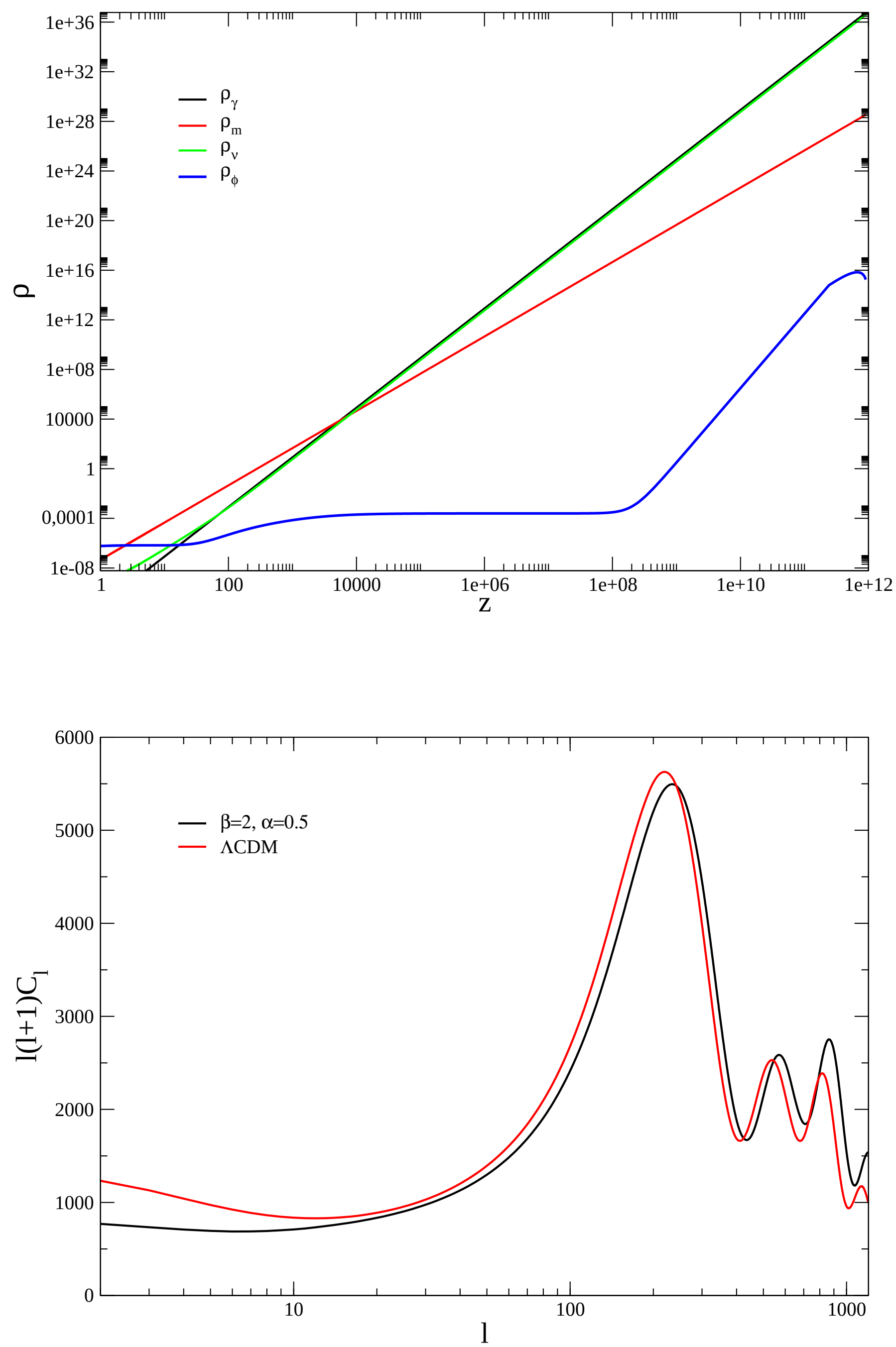

Figure 7.1 — A simple coupled model that can account for both CMB anisotropies and scalar field domination. We used the parameter combination $\beta = 2$, $\alpha = 0.5$. The initial conditions were fine-tuned to $\phi_0 = -0.5M_p$.

7.1.2 Variable Coupling

Another interesting developement of this simplest coupled neutrino model may be realized including the more general case of a time-dependent coupling.

As a matter of fact, we already wrote most of the equations for the evolution of the background and neutrino overdensities (like 4.11, 4.27) for the general case of $\beta(\phi)$, so that the calculations in this new model might be made quite straightforwardly.

Field dependent couplings were already proposed for dark matter-dark energy interactions [2], [55]; in the case of the coupled neutrino scenario, Christof Wetterich (see [71]) motivated a β of the form:

$$\beta(\phi) = \hat{\beta} + \frac{d\hat{\beta}}{d\ln(\phi)} \tag{7.1}$$

within a particle physics model.

7.1.3 Non-Degenerate Neutrino Masses

In our model we have always considered three neutrinos with degenerate masses, i.e. $m_1 \simeq m_2 \simeq m_3$. This assumption could be in principle relaxed, introducing a different coupling for every non degenerate neutrino mass, of the form:

$$m_{\nu_i}(\phi) = m_{\nu_i}^{(0)} e^{\beta_i(\phi)\frac{\phi}{M_p}} \tag{7.2}$$

It is reasonable to assume that in the case of a strong neutrino mass hierarchy, substantial changes (mainly due to the three different times in which neutrinos enter the non-relativistic regime) can affect the evolution of δ_νs. Neutrino mass mixing effects could also play an interesting role in this scenario.

Appendix A

CMBEASY

A.1 Program Overview

The C++ Boltzmann-code CMBEASY [17] has been developed by Michael Doran, Christian Mueller and Georg Robbers as an object oriented version of the well known program CMBFAST. It hasn't been written from scratch, although most of the code has been rewritten in order to benefit from the redesign [29]. The modularity of the program ensures that each part of the code can be tested and modified indipendently, an extremely useful feature for cosmological computing: new models or modifications of the elder ones can be easily implemented making use of the properties of *inheritance* and without need to know any detail about the rest of the program.

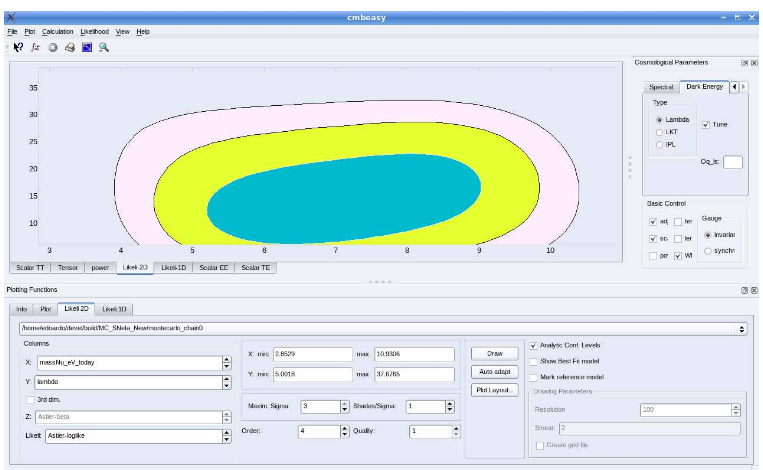

Figure A.1 — A screenshot of CMBEASY's graphical user interface

The program comes with a graphical user interface (GUI) which can be used for plotting results and also for data analysis. The GUI is based on the freely available Trolltech QT libraries [66]. The latest release of CMBEASY allows to compute background quantities as well as perturbative ones (like CMB and matter power spectra) for universes with baryons, dark matter, neutrinos, photons and different kinds of dark energy like cosmological constant and quintessence. The latter can have different features like inverse power law (IPL) or exponential potentials and leaping kinetic terms (LKT).

The program can be run from command line (allowing a high degree of customization through the configuration file *configuration.cfg*) or directly from the GUI, where only the basic settings can be user-defined.

A.2 Design

As previously stated, the CMBEASY makes a large use of basic objetct oriented programming properties, as can be seen by looking at fig. A.2 where *modularity* and *inheritance* are shown to be largely used throughout the main classes of the code.

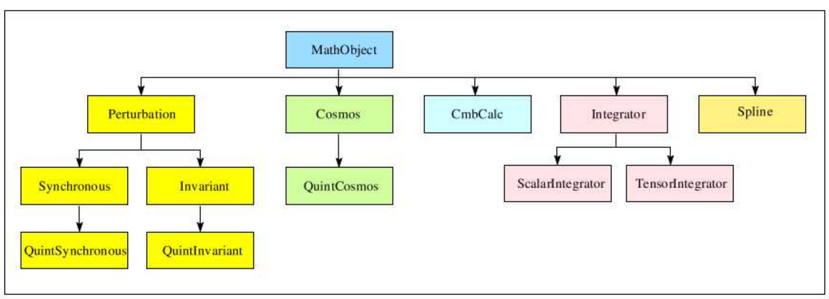

Figure A.2 — Hierarchy of the main classes of CMBEASY

All classes dealing with mathematics inherit from the MathObject from technical reasons. Then we have the Cosmos class, which calculates the evolution of background quantities: object-oriented programming allows us to easily extend it to subclasses (such as QuintCosmos) which take into account different scenarios. Perturbation equations are encapsulated in the Perturbation class, which implements two different gauges as subclasses. We then have the CmbCalc class, which is the central instance invoking Cosmos, Perturbation and Integrator classes in order to be able to calculate the CMB anisotropy spectrum.

In addition to the previously mentioned ones, we have a large set of other smaller classes, some of them (like the ControlPanel) holding common settings and some others providing additional mathematical functions (like the MiscMath class).

A.3 CMB Spectrum Calculation

In order to calculate the CMB anisotropy spectrum we have to:

(a) solve the expansion and thermal background evolution

(b) propagate the perturbation equations in Fourier space

(c) map the temperature anisotropy into the sky today

The core class CmbCalc implements these three steps, scheduling the call of other objects. The first step is achieved by the Cosmos class, which provides background quantities as $\rho_i(\tau), \Omega_i(a)$ where $i = \nu, \gamma, \phi$. Different background cosmologies can be easily implemented, inheriting from the Cosmos class and modifying only small portions of the code, as most of it is completely indifferent to the precise mechanism causing acceleration.

Then we have to compute fluctuations: this task is carried by the Perturbations class, most notably, we can perform calculations in different gauges using the various sub-classes which inherit from it. Perturbations determine the sources of CMB anisotropies: these sources are then convoluted with Bessel functions using the ScalarIntegrator sub-class to give us the C_l coefficients.

A.4 The *Analyze This!* package

In order to compute likelihoods and be able to constrain parameters, the CMBEASY code comes with an additional software [23] that allows such operations to be performed, the *Analyze This!* package. This is composed of two main parts: a MCMC driver, using LAM/MPI for parallel execution of chains, and the AnalyzeThis class, which evaluates likelihoods with respect to given data sets (such as WMAP, ACBAR, SDSS, 2dFGRS, SNIa compilations by Riess, Tonry and many others). Different sets can be easily added.
The MCMC driver consists of two routines: master() and slave(), allowing up to ten slave() and one master() routines to be started using LAM/MPI [50]. The master() determines the initial starting position of each chain,

sending the parameters to the slave()s and collecting the results and stores parameters and likelihoods whenever a step is accepted.
The AnalyzeThis class provides routines concerning CMB, SNe Ia and LSS measurements as well as tool for marginalizing and plotting MC output data.

Appendix B

Monte Carlo Markov Chains

Monte Carlo Markov Chain methods are an efficent way to explore the parameter space of a given model, since it depends only linearly on the number of parameters whereas n-dimensional grids depend on them exponentially. We'll now review briefly the basic ideas of MCMC simulations.

First of all, suppose that we are given a vector Θ containing all model's parameters and some observed data X; $L(X|\Theta)$ is the likelihood to observe X given Θ so that, specifying a prior distribution $P(\Theta)$ for the parameters, Bayes' theorem yields:

$$\pi(\Theta|X) = \frac{P(\Theta)L(X|\Theta)}{\int P(\Theta)L(X|\Theta)d\Theta} \tag{B.1}$$

where the function $\pi(\Theta|X)$ is the posterior distribution, which can be used to compute expectation values and confidence levels.

The idea of the MCMC method is to sample the posterior distribution $\pi(\Theta|X)$ in order to estimate its statistical properties: this can be accomplished using a Markov Chain, i.e. a stochastic process $\{\Theta_0, \Theta_1 ... \Theta_n\}$ where Θ_i only depends on Θ_{i-1}.
We want to choose the next point in the chain based on the previous point so that $\pi(\Theta|X)$ becomes the stationary distribution of the chain:

$$Dist\{\Theta_0, ..., \Theta_n\} \rightarrow \pi(\Theta|X), \quad n \rightarrow \infty \tag{B.2}$$

Even though there are many different ways to accomplish this, we will concentrate on the Metropolis algorithm, which is also the one used in the CMBEASY package.

B.1 The Metropolis Algorithm

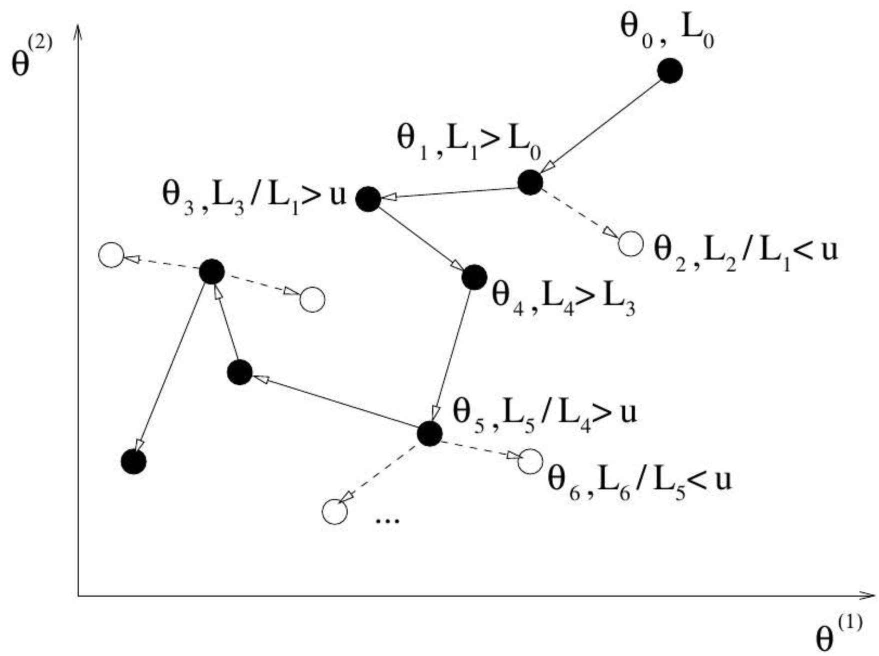

Figure B.1 — The Metropolis algorithm for two parameters: filled circles are points accepted by the chain while the empty ones are proposed but rejected points [23].

The global version of the Metropolis algorithm (the original one is the one presented in [57]), where all parameters change with every step, goes as follows:

(a) Choose a starting parameter vector Θ_0

(b) Compute the likelihood $L_0(X|\Theta_0)$

(c) Get a new parameter vector Θ_i sampling from a "proposal distribution"

(d) Compute $L_i(X|\Theta_i)$

(e) If $L_i > L_{i-1}$ save Θ_i and go back to (c)

(f) If $L_i < L_{i-1}$ generate a random variable u from $[0, 1]$. If $u < L_i/L_{i-1}$ take the step, otherwise reject it. Then, go back to (c) and start the whole procedure again.

This algorithm assumes flat priors $P(\Theta)$, it also assigns likelihood zero to any parameter set having at least one point outside of its prior.
Every chains starts randomly picking values from every parameter's interval, the second point then depends on the step size (which is set by the user) which determines it coordinates in the parameter space. This procedure is repeated for every point; the initial step size can be fixed or vary in order to ensure a better exploration of the parameter space. The latter procedure is implemented by CMBEASY using a so called *adaptive step size* algorithm.

B.2 Convergence Testing

At the beginning, the chain moves from Θ_0 into regions of higher likelihood. Points taken during this initial "burn-in" phase do not sample $\pi(\Theta|X)$ and therefore should be eliminated. Since it is difficult, at least in principle, to tell whether a single chain has converged towards $\pi(\Theta|X)$, we use several different chains with random starting points. Then, we monitor mixing and convergence using the test of Gelman and Rubin [42], which works as follows. We label by ψ_{ij} one entry of the parameter vector Θ at a point $j = 1, ..., n$ in the chain i; $\bar{\psi}_i$ is the mean for the chain i and $\bar{\psi}$ denotes the mean of all chains. The variance between the chains B and the variance within the single chain W are given by:

$$B = \frac{n}{m-1} \sum_{i=1}^{m} (\bar{\psi}_i - \bar{\psi})^2, \tag{B.3}$$

$$W = \frac{1}{m} \sum_{i=1}^{m} s_i^2, \quad s_i^2 = \frac{1}{n-1} \sum_{j=1}^{n} (\psi_{ij} - \bar{\psi}_i)^2 \tag{B.4}$$

and the quantity:

$$R = \frac{\frac{n-1}{n} W + \frac{1}{n} B}{W} \tag{B.5}$$

should converge to one. A value of $R < 1.2$ for all parameters indicates that the chain is sampling from $\pi(\Theta|X)$, and therefore, from this point onwards, points can be used for parameter estimates. In CMBEASY this also *freezes* the step size to a fixed value, suspending the adaptive algorithm. The exact number of points necessary for a good sampling of the parameter space usually depends on the model, the used data set and the desired accurracy. This is the reason why in CMBEASY the MCMC simulation runs indefinitly, although a "breaking" criterion may be introduced at user's will.

Appendix C

Scaling Solutions in a General Background

We will now derive the general conditions for the existence of scaling solutions given a general cosmologic background. To do so, we consider an action of the form:

$$S_{tot} = \int d^4x\sqrt{-g}[\rho(X,q) + \frac{1}{2}M_{pl}^2 R] + S_m(\phi) \tag{C.1}$$

where $X = -\frac{1}{2}g^{\mu\nu}\partial_\mu\phi\partial_\nu\phi$ is the standard kinetic term.

We assume that the general form of the first Friedmann equation holds:

$$H^2 = \beta_n^2\rho_T^n \tag{C.2}$$

Now, considering the case of a single dominant component and a subdominant scalar field, and allowing the two fluids to interact (we can easily recover the uncoupled case simply letting $Q \to 0$), we write the continuity relations:

$$\begin{aligned} \frac{d\rho_\phi}{dN} + 3(1+w_\phi)\rho_{phi} &= -Q\rho_m\frac{d\phi}{dN}, \\ \frac{d\rho_m}{dN} + 3(1+w_m)\rho_m &= Q\rho_m\frac{d\phi}{dN}. \end{aligned} \tag{C.3}$$

From the scaling condition $\rho_\phi/\rho_m = C$ we have that:

$$\ln\rho_\phi - \ln\rho_m = C' \tag{C.4}$$

which in turn implies:

$$\frac{d\ln\rho_\phi}{dN} = \frac{d\ln\rho_m}{dN} \tag{C.5}$$

Substituting into this last relation the equations C.3 we obtain:

$$\frac{d\phi}{dN} = \frac{3\Omega_\phi}{Q}(w_m - w_\phi) = const. \tag{C.6}$$

that, using again the C.3, gives us:

$$\begin{aligned}\frac{d\ln\rho_\phi}{dN} &= 3\left[-(1+w_m) + \frac{\rho_\phi}{\rho_\phi+\rho_m}(w_m - w_\phi)\right] \\ &= \frac{-(1+w_m)(\rho_m+\rho_\phi) + \rho_\phi(w_m - w_\phi)}{\rho_m+\rho_\phi} \\ &= -3(1+w_{eff})\end{aligned} \tag{C.7}$$

where w_{eff} is:

$$w_{eff} = \frac{w_m\rho_m + w_\phi\rho_\phi}{\rho_m\rho_\phi} \tag{C.8}$$

a general model independent definition.

Looking back at our definition of X we see that:

$$2X = H^2\left(\frac{d\phi}{dN}\right)^2 \sim H^2 \sim \rho_T^n \tag{C.9}$$

which implies:

$$\frac{d\ln X}{dN} = -3n(1+w_{eff}) \tag{C.10}$$

so that, remembering $p_T = \rho_T w_T$, we have:

$$\frac{d\ln p_\phi}{dN} = -3(1+w_{eff}). \tag{C.11}$$

These last two relations, combined with equation C.6, give:

$$n\frac{d\ln p_\phi}{d\ln X} - \frac{1}{\lambda}\frac{d\ln p_\phi}{d\phi} = 1 \tag{C.12}$$

where:

$$\lambda = Q\left[\frac{1-\Omega_\phi(w_m - w_\phi)}{\Omega_\phi(w_m - w_\phi)}\right] \tag{C.13}$$

The equation C.12 has the following general solution [62]:

$$p_\phi(X,\phi) = X^{\frac{1}{n}} g(Xe^{n\lambda\phi}) \tag{C.14}$$

We can easily show that the variable $Y = Xe^{n\lambda\phi}$, on which the function g depends, is constant along the scaling solution; therefore, we have:

$$Xe^{n\lambda\phi} = Y_0 = const. \tag{C.15}$$

which in turn implies $p \sim X^{1/n}$. This result gives us the defining property of scaling solutions, i.e., that in this regime the Lagrangian and the pressure density depend upon the kinetic energy alone.

Appendix D

Gauge Choice in Cosmological Perturbation Theory

Introducing the cosmological standard model, we stated that the main assumption on which it relied was the *cosmological principle*, i.e. the assumption that the universe is homogeneous and isotropic. Of course, this cannot be on all scales: structures like planetary systems, galaxies and galaxy clusters are the most evident proof of the non-homogeneity of the universe.

Nonetheless, these inhomogeneities are well understood in the frame of the cosmological standard model; in particular, we can study how primordial small fluctuations (supposedly set at the end the *inflationary epoch*) grew until they clustered into complex structures to gravitational non linear phenomena.

We'll make here a concise description of cosmological perturbation theory. For a more in-depth analysis we refer to standard works on the subject, such as [54] as well as textbooks like [21]. The initial step in perturbation theory consists in perturbing the metric; at first order we have:

$$g_{\mu\nu} = g^{(0)}_{\mu\nu} + g^{(1)}_{\mu\nu}, \tag{D.1}$$

general relativity requires that this transformation leaves the line element:

$$ds^2 = g_{\mu\nu} dx^\mu dx^\nu \tag{D.2}$$

invariant with respect to a change in the coordinate system. Coordinate transformations of this type are called *gauge transformation*; the choice of the coordinate system (*gauge*) is not unique, and has to be made according to the specific problem we have to face.

The two most popular choices are the:

Newtonian Gauge : a coordinate transformation that leaves the *unperturbed* part of the metric tensor, $g^{(0)}_{\mu\nu}$ unchanged [59]

Synchronous Gauge : a system of coordinates in which all the observers share the same conformal time [53]

In addition to these two gauges, it is possible to introduce *gauge invariant* variables [8], [30], i.e. a set of variables, built as combinations of ordinary perturbative quantities like potentials Φ and density contrasts δ; which remain unchanged for arbitrary gauge transformations.

The line element in the *newtonian* gauge takes the form:

$$ds^2 = a^2(\tau)[(1+2\psi)d\tau^2 - (1-2\phi)dx_i dx^i] \tag{D.3}$$

whereas in the *synchronous* gauge we have:

$$ds^2 = a^2(\tau)(d\tau^2 - (\delta_{ij} - h_{ij})dx^i dx^j) \tag{D.4}$$

We notice that the metric in the newtonian gauge has a diagonal form, while in the synchronous one it has also non diagonal elements. Furthermore, since in the latter section we'll write our perturbed equations in the Fourier space, it turns out useful to explicitly write our spatial perturbation field for the synchronous gauge h_{ij}:

$$h_{ij}(\vec{x},\tau) = \int d^3k e^{i\vec{k}\cdot\vec{x}}[\hat{k}_i\hat{k}_j h(\vec{k},\tau) + (\hat{k}_i\hat{k}_j - \frac{1}{3}\delta_{ij})6\eta(\vec{k},\tau)] \tag{D.5}$$

where h and η are two scalar functions for the metric perturbations in this gauge.

Perturbation of the Evolution Equations

Once that the gauge has been chosen, we have to substitute our new perturbed metric into the Friedmann equations and the energy-momentum conservation relations. First of all, we rewrite the Friedmann equations in terms of the conformal time where the scale factor is $a = a(\tau)$:

$$\mathcal{H}^2 = \frac{8\pi a^2}{3}(\rho_{tot}) \tag{D.6}$$

$$\mathcal{H}' = -\frac{4\pi}{3}a^2(p_{tot} + 3\rho_{tot}) \tag{D.7}$$

while the conservation of the energy-momentum tensor T^{μ}_{ν} implies the vanishing of the covariant divergence, that can be written as:

$$T^{\mu}_{\nu;\mu} = T^{\mu}_{\nu,\mu} + \Gamma^{\alpha}_{\beta\alpha} T^{\beta}_{\nu} - \Gamma^{\alpha}_{\nu\beta} T^{\beta}_{\alpha} = 0 \tag{D.8}$$

The next step is writing the new Christoffel symbols Γ in terms of the perturbed metric, we recall that:

$$\Gamma^{\gamma}_{\alpha\beta} = \frac{1}{2} g^{\gamma\eta} (g_{\alpha\eta,\beta} + g_{\beta\eta,\alpha} - g_{\alpha\beta,\eta}) \tag{D.9}$$

which, substituting D.3, yields:

$$\begin{aligned}
\delta\Gamma^{0}_{ij} &= \delta_{ij}[2\mathcal{H}(\phi + \psi) + \dot{\phi}] \\
\delta\Gamma^{0}_{00} &= \dot{\psi} \\
\delta\Gamma^{0}_{0i} &= \delta\Gamma^{0}_{i0} = ik\phi/sqrt3 \\
\delta\Gamma^{i}_{j0} &= \delta^{i}_{j}\dot{\phi}
\end{aligned}$$

for the newtonian gauge; similar relations can be obtained the synchronous one, too. We can thus straightforwardly write our *continuity relation*:

Newtonian Gauge:

$$\begin{aligned}
\dot{\delta} &= -(1+w)(\Theta - 3\dot{\phi} - 3\frac{\dot{a}}{a}\left(\frac{\delta P}{\delta \rho} - w\right))\delta \\
\dot{\Theta} &= -\frac{\dot{a}}{a}(1-3w)\Theta - \frac{\dot{w}}{1+w}\Theta + \frac{\delta P/\delta\rho}{1+w}k^2\delta - k^2\sigma + k^2\psi
\end{aligned} \tag{D.10}$$

Synchronous Gauge:

$$\begin{aligned}
\dot{\delta} &= -(1+w)\left(\Theta + \frac{\dot{h}}{2}\right) - 3\frac{\dot{a}}{a}\left(\frac{\delta P}{\delta \rho} - w\right)\delta \\
\dot{\Theta} &= -\frac{\dot{a}}{a}(1-3w)\Theta - \frac{\dot{w}}{1+w}\Theta + \frac{\delta P/\delta\rho}{1+w}k^2\delta - k^2\sigma
\end{aligned} \tag{D.11}$$

and the Friedmann equations :

Newtonian Gauge:

$$\begin{aligned} k^2\phi + 3\mathcal{H}(\dot{\phi} + \mathcal{H}\psi) &= -4\pi a^2 \rho\delta \\ k^2(\dot{\phi} + \mathcal{H}\psi) &= 4\pi a^2 \Theta\rho \\ \phi &= \psi \end{aligned} \tag{D.12}$$

Synchronous Gauge:

$$\begin{aligned} \mathcal{H}\dot{h} &= 2k^2\eta + 8\pi a^2 \delta T^0_0 \\ \dot{\eta} &= -4\pi \frac{a^2}{k^2} i k^i \delta T^0_i \\ \ddot{h} &= \mathcal{H}\dot{h} + 8\pi a^2(\delta T^0_0 - \delta T^i_i) \end{aligned} \tag{D.13}$$

for both the newtonian and synchronous gauges, in the Fourier space; where we have denoted with Θ the fluid velocity divergence, $\nabla^i v_i$.

Relation between the Two Gauges

We can obtain the relations connecting perturbative quantities in the two gauges remembering that the energy-momentum tensor in the synchronous gauge $T^{\mu}_{(s)\nu}$ (with coordinates y^{μ}) is related to the one in the newtonian gauge $T^{\mu}_{(n)\nu}$ (with coordinates x^{μ}) by the transformation:

$$T^{\mu}_{(s)\nu} = \frac{\partial y^{\mu}}{\partial x^{\alpha}} \frac{\partial x^{\beta}}{\partial y^{\nu}} T^{\alpha}_{(n)\beta} \tag{D.14}$$

which yields:

$$\begin{aligned} \delta_{(s)} &= \delta_{(c)} - \alpha \frac{\dot{\rho}_{tot}}{\rho_{tot}} \\ \Theta_{(s)} &= \Theta_{(c)} - \alpha k^2 \\ \delta P_{(s)} &= \delta P_{(c)} - \alpha \dot{P}_{tot} \end{aligned}$$

if we evaluate these perturbations at the same spacetime coordinate value.

Bibliography

[1] N. Afshordi, M. Zaldarriga, and K. Kohri. Instability of Dark Energy with Mass-Varying Neutrinos. *Phys. Rev. D*, 72, 2005.

[2] L. Amendola, D. Tocchini-Valentini, C. Ungarelli, and M. Gasperini. Early Acceleration and Adiabatic Matter Perturbations in a Class of Dilatonic Dark Energy Models. *Phys. Rev. D*, 67, 2002. astro-ph/0208032.

[3] L. Amendola, C. Wetterich, and M. Baldi. Quintessence Cosmologies with a Growing Matter Component. *Phys. Rev. D*, 78, 2008. astro-ph/07063064.

[4] Luca Amendola. Scaling Solutions In General Nonminimal Coupling Theories. *Phys. Rev. D*, 60, 1999.

[5] Luca Amendola. Coupled Quintessence. *Phys. Rev. D*, 62, 2000.

[6] N.A. Arhipova, T. Kahniashvili, and V.N. Lukash. Abundance and Evolution of Galaxy Clusters in Cosmological Models with Massive Neutrinos. *Astron. Astrophys.*, 386, 2002. astro-ph/0110426.

[7] M. Baldi, V. Pettorino, G. Robbers, and V. Springel. N-Body Simulations of Coupled Dark Energy Cosmologies. *Mon. Not. R. Astron. Soc.*, 2008. [astro-ph] arXiv:0812.3901.

[8] J.M. Bardeen. . *Phys. Rev. D*, 22, 1980.

[9] M. Bartelmann, M. Doran, and C. Wetterich. Non-linear Structure Formation in Cosmologies with Early Dark Energy. *Astron. Astrophys.*, 454, 2005. astro-ph/0507257.

[10] G. Bhattacharyya, H. Paes, and T.J. Weiler. Particle Physics Implications of the WMAP Neutrino Mass Bound. *Phys. Lett. B*, 564, 2003. hep-ph/0302191.

[11] O.E. Bjaelde, A.W. Brookfield, C. van de Bruck, S. Hannestad, D.F. Mota, L. Schrempp, and D. Tocchini-Valentini. Neutrino Dark Energy - Revisiting the Stability Issue. *JCAP*, 026, 2008. [astro-ph] arXiv:0705.2018.

[12] C.G. Boehmer, G. Caldera-Cabral, R. Lakzoz, and R. Maartens. Dynamics of Dark Energy with a Coupling to Dark Matter. *Phys. Rev. D*, 78, 2008. [gr-qc] arXiv:0801.1563.

[13] A.W. Brookfield, C. van de Bruck, D.F. Mota, and D. Tocchini-Valentini. Cosmology with Massive Neutrinos Coupled to Dark Energy. *Phys. Rev. Lett.*, 96, 2006.

[14] N. Brouzakis, N. Tetradis, and C. Wetterich. Neutrino Lumps in Quintessence Cosmology. *Phys. Lett. B*, 665, 2008. [astro-ph] arXiv:0711.2226.

[15] Y.C. Cai, S. Cole, A. Jenkins, and C. Frenk. Towards an Accurate Modelling of the ISW Effect the Nonlinear Contribution, 2008. [astro-ph] arXiv:0809.4488.

[16] R.R. Caldwell, C. Wetterich, G. Schaefer, C. Mueller, and M. Doran. Early Quintessence in Light of WMAP. *Astrophys. J.*, 591, 2003. astro-ph/0302505.

[17] Cmbeasy. http://www.cmbeasy.org.

[18] E.J. Copeland, A.R. Liddle, and D. Wands. Exponential Potentials and Cosmological Scaling Solutions. *Phys. Rev. D*, 4686, 1997.

[19] E.J. Copeland, M. Sami, and S. Tsujikawa. Dynamics Of Dark Energy. *Int. J. Mod. Phys. D*, 15, 2006. hep-th/060305.

[20] P.S. Corasaniti, M. Kunz, D. Parkinson, E.J. Copeland, and B.A. Basset. The Foundations of Observing Dark Energy Dynamics with the Wilkinson Microwave Anisotropy Probe. *Phys. Rev. D*, 70, 2004. astro-ph/0406608.

[21] Scott Dodelson. *Modern Cosmology.* Addison-Wesley, 2004.

[22] M. Doran, K. Karwan, and C. Wetterich. Observational Constraints on the Dark Energy Density Evolution. *JCAP*, 007, 2005. astro-ph/0508132.

[23] M. Doran and C.M. Mueller. Analyze This! A Cosmological Constraint Package for CMBEASY, 2004. astro-ph/0311311.

[24] M. Doran and G. Robbers. Early Dark Energy Cosmologies. *JCAP*, 026, 2006. astro-ph/0601544.

[25] M. Doran, G. Robbers, and C. Wetterich. Impact of Three Years of Data from the Wilkinson Microwave Anisotropy Probe on Cosmological Models with Dynamical Dark Energy. *Phys. Rev. D*, 75, 2007.

[26] M. Doran and C. Wetterich. Quintessence and the cosmological constant. In *Dark Matter 2002*, 2002. astro-ph/0205267.

[27] M. Doran, C. Wetterich, M. Liley, and J. Schwindt. Quintessence and the Separation of the Cosmic Microwave Background Peaks. *Astrophys. J.*, 559, 2001.

[28] Michael Doran. A Primer on Cosmology and the Cosmic Microwave Background. www.cmbeasy.org.

[29] Michael Doran. CMBEASY: an object oriented code for the Cosmic Microwave Background. *astro-ph/0302138*, 2006.

[30] R. Durrer. . 1993. ZU-TH14/92.

[31] A.G. Riess *et al.* Observational Evidence from Supernovae for an Accelerating Universe and a Cosmological Constant. *Astron. J.*, 116, 1998.

[32] A.G. Riess *et al.* BVRI Light Curves for 22 Type Ia Supernovae. *Astron. J.*, 117, 1999. astro-ph/9810291.

[33] A.G. Riess *et al.* Type Ia supernovae discoveries at $z > 1$ from the Hubble Space Telescope: Evidence for Past Acceleration and Constraints on Dark Energy Evolution. *Astrophys. J.*, 607, 2004. astro-ph/0402512.

[34] C. Weinheimer *et. al.* High Precision Measurement of the Tritium β Spectrum Near its Endpoint and Upper Limit on the Neutrino Mass. *Nucl. Phys. B*, 118, 1999.

[35] E.V. Linder *et. al.* Looking Beyond ΛCDM with the Union Supernovae Compilation, 2008. [astro-ph] arXiv:0807.1108.

[36] J. Bonn *et. al.* The Mainz Neutrino Mass Experiment. *Nucl. Phys. B*, 91, 2001.

[37] L. Baudis *et. al.* Limits on the Majorana Neutrino Mass in the 0.1 eV Range. *Phys. Rev. Lett.*, 83, 1999.

[38] M. Kowalski *et al.* Improved Cosmological Constraints from New, Old and Combined Supernova Datasets. *Astrophys. J.*, 686, 2008. [astro-ph] arXiv:0804.4142.

[39] T.M. Davis *et al.* Observational Constraints on the Nature of Dark Energy: First Cosmological Results from the ESSENCE Supernova Survey. *Astrophys. J.*, 666, 2007.

[40] R. Fardon, A.E. Nelson, and N. Weiner. Dark Energy From Mass Varying Neutrinos. *JCAP*, 0410, 2004.

[41] M. Fukugita, K. Ichikawa, M. Kawasaki, and O. Lahav. Limit on the Neutrino Mass from the WMAP Three Year Data. *Phys. Rev. D*, 74, 2006. astro-ph/0605362.

[42] A. Gelman and D.B. Rubin. Inference from Iterative Simulation Using Multiple Sequences. *Statist. Sci.*, 7, 1992.

[43] Mathias Grany. Quintessence and Quantum Corrections. Master's thesis, Technische Universitaet Muenchen, 2004.

[44] A. Hebecker and C. Wetterich. Natural Quintessence? *Phys. Lett. B*, 497, 2001. hep-ph/0008205.

[45] G. Huey and B.D. Wandelt. Interacting Quintessence, the Coincidence Problem and Cosmic Acceleration. *Phys. Rev. D*, 74, 2006.

[46] P. Q. Hung. Sterile Neutrino and Accelerating Universe, 2000. hep-ph/0010126.

[47] K. Ichik and Y.Y. Keum. Neutrino Masses from Cosmological Probes in Interacting Neutrino Dark Energy Models. *JHEP*, 58, 2008. [hep-ph] arXiv:0803.2274v3.

[48] E. *et. al.* Komatsu. Five-Year Wilkinson Microwave Anisotropy Probe (WMAP) Observations: Cosmological Interpretation. *Astrophys. J. Suppl.*, 180, 2008. [astro-ph] arXiv:0803.0547.

[49] J.R. Kristiansen, H.K. Eriksen, and O. Elgaroey. Revised WMAP Constraints on Neutrino Masses and Other Extensions of the Minimal ΛCDM Model. *Phys. Rev. D*, 74, 2006.

[50] Open System Labs. www.lam-mpi.org.

[51] R. Lazkoz, S. Nesseris, and L. Perivolaropoulos. Exploring Cosmological Expansion Parametrizations with the Gold SnIa Dataset. *JCAP*, 010, 2005. astro-ph/0503230.

[52] J. Lesgourgues and S. Pastor. Massive Neutrinos and Cosmology. *Phys. Rept.*, 429, 2006. astro-ph/0603494.

[53] E.M. Lifshitz. *J. Phys. USSR*, 10, 1946.

[54] C.P. Ma and E. Bertschinger. Cosmological Perturbation Theory in the Synchronous and Conformal Newtonian Gauges. *Astrophys. J.*, 445, 1995. astro-ph/9506072.

[55] R. Mainini and S. Bonometto. Limits on Coupling between Dark Components. *JCAP*, 020, 2007. astro-ph/0703303.

[56] G. Mangano, G. Miele, and V. Pettorino. Coupled Quintessence and the Coincidence Problem. *Mod. Phys. Lett.*, A18, 2003. astro-ph/0212518.

[57] N. Metropolis, A.W. Rosenbluth, M.N. Rosenbluth, A.H. Teller, and E. Teller. Equation of State Calculation by Fast Computing Machines. *J. Chem. Phys.*, 21, 1953.

[58] D.F. Mota, V. Pettorino, G. Robbers, and C. Wetterich. Neutrino Clustering in Growing Neutrino Quintessence. *Phys. Lett. B*, 663, 2008. astro-ph/08021515.

[59] V.F. Mukhanov, H.A. Feldman, and R. Brandenberger. . *Phys. Rep.*, 215, 1992.

[60] S. *et al.* Perlmutter. Measurements of Omega and Lambda from 42 High-Redshift Supernovae. *Astrophys. J.*, 517, 1999.

[61] V. Pettorino, D.F. Mota, G. Robbers, and C. Wetterich. Clustering in Growing Neutrino Cosmologies. In *DSU 2008*, 2009. [astro-ph] arXiv:0901.1239.

[62] F. Piazza and S. Tsujikawa. Dilatonic Ghost Condensate as Dark Energy. *JCAP*, 0407, 2004.

[63] B. Ratra and P. Peebles. Cosmological Consequences of a Rolling Homogeneous Scalar Field. *Phys. Rev. D*, 37, 1988.

[64] R.K. Sachs and A.M. Wolfe. Perturbations of a Cosmological Model and Angular Variations of the Microwave Background. *Astrophys. J.*, 147, 1967.

[65] Anzhe Slosar. Detecting Neutrino Mass Difference with Cosmology. *Phys. Rev. D*, 73, 2006. astro-ph/0602133.

[66] Trolltech. QT-Library. www.trolltech.com.

[67] Steven Weinberg. The Cosmological Constant Problems. In *Dark Matter 2000*, 2000. astro-ph/0005265.

[68] Christof Wetterich. Cosmologies With Variable Newton's Constant. *Nucl. Phys. B*, 302, 1988.

[69] Christof Wetterich. The Cosmon Model For An Asymptotically Vanishing Time-Dependent Cosmological Constant. *Astron. Astrophys. J.*, 301, 1995.

[70] Christof Wetterich. Phenomenological Parametrization of Quintessence. *Phys. Lett. B*, 594, 2004. astro-ph/0403289.

[71] Christof Wetterich. Growing Neutrinos and Cosmological Selection. *Phys. Lett. B*, 655, 2007. hep-ph/07064427.

[72] Christof Wetterich. Naturalness of Exponential Cosmon Potentials and the Cosmological Constant Problem. *Phys. Rev. D*, 77, 2008. hep-th/08013208.

[73] N. Wintergerst and V. Pettorino. Hydrodinamical Equations for a Spherically Symmetric Neutrino Overdensity. Private Communication, 2008.

[74] Wen Zhao. Attractor Solution in Coupled Yang-Mills Field Dark Energy Models. *IJMPD*, 2008. [gr-qc] arXiv:0810.5506.

[75] C. Zunckel and P.G. Ferreira. Conservative Estimates of the Mass of the Neutrino from Cosmology. *JCAP*, 004, 2007. astro-ph/0610597.